JOURNAL OF GEOPHYSICAL RESEARCH, VOL. 103, NO. B10, PAGES 24,201–24,221, OCTOBER 10, 1998

Axial magnetic anomaly amplitude along the Mid-Atlantic Ridge between 20°N and 40°N

Morgane Ravilly, Jérôme Dyment, Pascal Gente, and Rémy Thibaud

Centre National de la Recherche Scientifique, Unité Mixte de Recherche "Domaines Océaniques"
Institut Universitaire Européen de la Mer, Université de Bretagne Occidentale, Plouzané, France

Abstract. After reduction to correct for the topography, spreading rate, latitude, and lineation azimuth effects, axial magnetic anomalies amplitudes are compared with bathymetric, gravity, seismological, and geochemical data along a 2600-km-long section of the Mid-Atlantic Ridge axis between 20°N and 40°N. Significant results are obtained at two different scales, a regional one (> 100 km) related to sublithospheric thermal perturbations such as those associated to hotspots and a local one (< 100 km) related to ridge segmentation. At a regional scale, two long-wavelength highs of the axial magnetic anomaly amplitudes are observed between 37.5°N and 40°N and between 27°N and 30°N. The first high, associated with marked bathymetric, gravity, geoid, seismic velocity, and geochemical anomalies, is related to the Azores hotspot and is interpreted as reflecting the existence of a thick and/or Fe-Ti enriched magnetic source layer. A second long-wavelength high centered at 28.5°N corresponds to a weaker bathymetric and gravity signature; it is associated with a large low seismic velocity anomaly and a marked intermediate-wavelength positive geoid high which suggest higher sublithospheric temperatures, deeper and more extensive partial melting, and a thicker and/or Fe-Ti enriched magnetic source layer. At a local scale, all but one of the 25 ridge segments investigated show that axial magnetic anomaly amplitude is higher at segment ends by a factor of 2 compared to segment centers. A clear correlation is observed between the range of axial magnetic anomaly amplitude and the range of the mantle Bouguer anomaly (ΔMBA) within each segment. More complex relationships exist between median amplitude, amplitude at segment centers and at segments ends, and ΔMBA. Separation of segments in two groups ("hotter" and "colder") based on ΔMBA shows different types of variations among segment, with grouped amplitudes at segment centers and scattered amplitudes at segment ends for hotter segments and the opposite for colder segments. These observations support shallow fractionation and the presence of serpentinized bodies in the vicinity of discontinuities as the major processes which control the axial magnetic anomaly amplitude variations.

1. Introduction

Within the framework of the magnetic telechemistry hypothesis [*Vogt and Johnson,* 1973], the amplitude of marine magnetic anomalies is directly related to the geochemistry of the oceanic crust and seafloor spreading processes: extensive fractionation results in high iron oxide content, Fe-Ti-enriched basalts, and therefore high magnetic anomaly amplitudes [*Vogt,* 1979]. This hypothesis was initially formulated to account for the observation of seafloor provinces with high-amplitude magnetic anomalies [*Vogt,* 1979; *Anderson et al.,* 1980]. At a regional scale, several hotspots show the association of high magnetic anomaly amplitudes with Fe-Ti-rich basalts derived from a hotspot source, such as the Galapagos and Iceland hotspots [*Vogt and Johnson,* 1973; *Schilling et al.,* 1976; *Vogt and DeBœr,* 1976; *Vogt,* 1979]. Various data, including gravity [*Detrick et al.,* 1995; *Thibaud et al.,* this issue], bathymetry [*Gente,* 1995; *Thibaud et al.,* this issue], and geochemistry [*Klein and Langmuir,* 1989; *Dosso et al.,* 1993] show a strong influence of the Azores hotspot on the Mid-Atlantic Ridge (MAR). The magnetic signature of this hotspot is one focus of this study.

More recent investigations at the scale of ridge segments seem to support the magnetic telechemistry hypothesis. Along fast and intermediate spreading centers in the Pacific Ocean, high axial magnetic anomaly amplitudes, equivalent magnetization, i.e., computed from the anomalies following the *Parker and Huestis* [1974] method, and rock magnetization intensities are observed at the tip of ridge segments and near propagating ridges [*Detrick and Lynn,* 1975; *Sempéré,* 1991;

Paper number 98JB01071.
0148-0227/98/98JB-01071$09.00

Carbotte and Macdonald, 1992; *Tivey,* 1994]. The high magnetizations are generally associated with Fe-Ti-rich basalts resulting from shallow fractionation in small magma bodies [*Vogt,* 1979; *Christie and Sinton,* 1981]. In the Atlantic Ocean, magnetic anomaly amplitude and equivalent magnetization intensity increase at segment ends at various locations along the slow spreading MAR, between 28°N and 31°N [*Pariso et al.,* 1996], 25°45'N and 26°30'N (TAG area [*Tivey et al.,* 1993]), 24°N and 24°40'N [*Hussenoeder et al.* 1996], 20°N and 24°N [*Pockalny et al.,* 1995], and 31°S and 35°S [*Weiland and Macdonald,* 1993; *Weiland et al.,* 1996]. The correlation between iron oxide content and magnetic anomaly amplitude [*Weiland and Macdonald,* 1993; *Weiland et al.,* 1996] suggests that the high magnetic anomaly amplitudes at segment ends result from the presence of Fe-Ti-rich basalts. However, spreading processes at slow ridges are essentially three-dimensional [*Lin et al.,* 1990; *Tolstoy et al.,* 1993; *Gente et al.,* 1995], and magma chambers, if any, are transient features [*Lagabrielle and Cannat,* 1990; *Detrick et al.,* 1995; *Calvert,* 1995; *Cannat,* 1996] in which fraction-

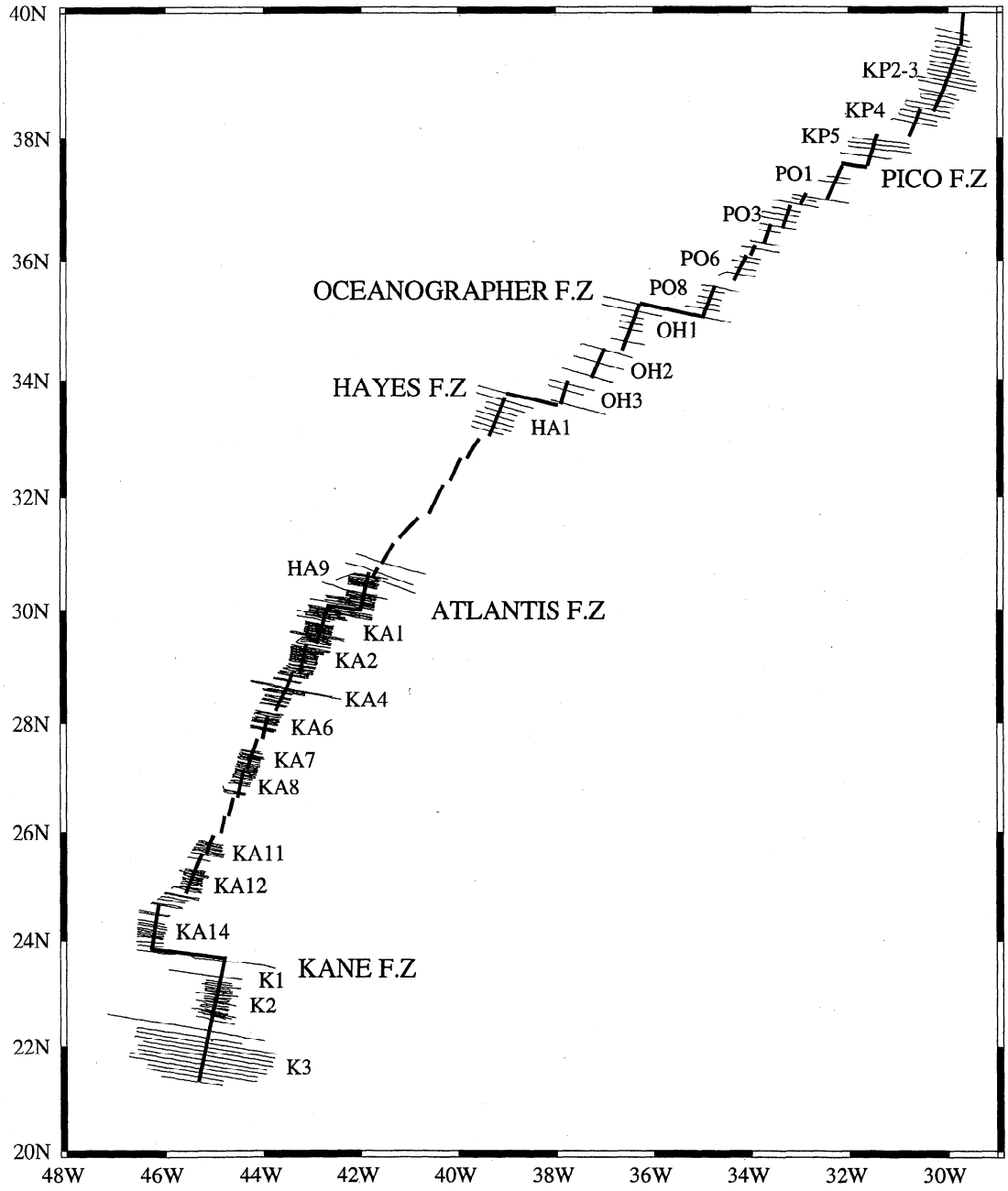

Figure 1. Location of the surface total magnetic field profiles extracted from the Geodas and Sismer bases data across the ridge axis between 20°and 40°N. The selection includes only profiles perpendicular (± 20°) to the ridge (schematized with thick lines) which display the whole axial magnetic anomaly.

ation does not seem to be an important process [*Niu and Batiza,* 1994]. So various other explanations have been proposed to account for the observed increase of magnetic anomaly amplitude at segment ends: outcrops of serpentinized peridotites along the traces of second-order discontinuities [*Pockalny et al.,* 1995; *Pariso et al.,* 1996], thickness variation of the magnetic source layer [*Grindlay et al.,* 1992; *Tivey et al.,* 1993; *Pariso et al.,* 1996], and decrease of magnetization at the segment center related to more pervasive faulting [*Tivey and Johnson,* 1987] or to hydrothermal activity [*Tivey and Johnson,* 1987; *Wooldridge et al.,* 1992].

In this paper, we investigate the amplitudes of axial magnetic anomaly along a 2600-km-long section of the MAR located between 20°N and the Azores platform near 40°N. This area is of particular interest because it provides an opportunity to study the magnetic signature of a hotspot and of ridge segments with relatively dense data coverage. The ridge segments are characterized by an average length of 50 km and variable morphology; they are separated by five transform faults (from north to south: Pico Fracture Zone (FZ), Oceanographer FZ, Hayes FZ, Atlantis FZ, and Kane FZ), and several second and third-order discontinuities [*Sempéré et al.,* 1990, 1993; *Gente et al.,* 1995; *Detrick et al.,* 1995; *Thibaud et al.,* this issue]. The major questions addressed by this study are as follows: (1) Is the Azores hotspot associated with a particular magnetic signature? (2) Does the amplitude of axial magnetic anomalies show a systematic variation within the 10-100 km segmentation scale? (3) Which processes control this variation (petrologic and geochemical segmentation, thermal structure, thickness variation of the magnetic source layer, contribution of serpentinized peridotites, low-temperature alteration, hydrothermalism)?

2. Data Processing

About 400 total magnetic field profiles and the associated bathymetry were selected from two marine geophysical bases data, Geodas (National Geodetic Data Center (NGDC), Boulder, Colorado) and Sismer (Ifremer, Brest, France). Data coverage across the MAR axial magnetic anomaly is satisfactory between 21°-31°N and 34°-39°40'N, with profiles 1-11 km apart. A lack of data exists between 31°and 33°N (Figure 1). Profiles which do not present a clear axial magnetic anomaly are rejected, as for instance at the extreme tip of ridge segments where the anomalies are strongly affected by three-dimensional (3-D) effects. Figure 2 presents the steps of data processing. The regional field has been removed using the International Geomagnetic Reference Field (IGRF) model for the appropriate year and location for each profile. Profiles are projected along the spreading direction computed at each measurement point from the present-day Africa-North America rotation parameters [*Argus et al.,* 1989] and resampled at constant intervals of 0.9 km (Figure 2, curve A). Each profile is reduced to the pole (Figure 2, curve B) using the theta method of *Schouten and McCamy* [1972]. The direction of the ambient geomagnetic field is given by the appropriate IGRF model [IAGA Division V Working Group 8, 1996]; that of the magnetization is computed assuming a geocentric dipole parallel to the Earth axis. Lineation azimuths A are obtained from the rotation parameters of *Argus et al.* [1989].

In order to reduce the magnetic data for the effect of topography, equivalent magnetization is computed along the reducted to the pole (RTP) profiles by the iterative 2-D inversion method of *Parker and Huestis* [1974] assuming a 500-m-thick magnetic layer (Figure 2, curve C). This method tends to amplify both longer and shorter wavelengths [see, e.g., *Wittpenn et al.,* 1989]. Long wavelengths are either low-amplitude regional magnetic anomalies such as those observed by satellite [i.e., *Arkani-Hamed et al.,* 1994; *Ravat et al.,* 1995] or diurnal variations of the geomagnetic field; short wavelengths are related to instrumental and other types of noise. To reduce the amplification of longer and shorter wavelengths and to ensure convergence of the iterations, the equivalent magnetization solution is band-pass filtered at each iteration, with a wavelength band of 2.5 to 150 km. Still, the equivalent magnetization displays short-wavelength fluctuations superimposed on the main anomalies. They most likely result from geomagnetic intensity variations and short polarity reversals, local complexities in the spreading processes such as spreading asymmetry or small ridge jumps, enhancement of instrumental noise, or a combination of these effects. Whether real or fictitious, these local varia-

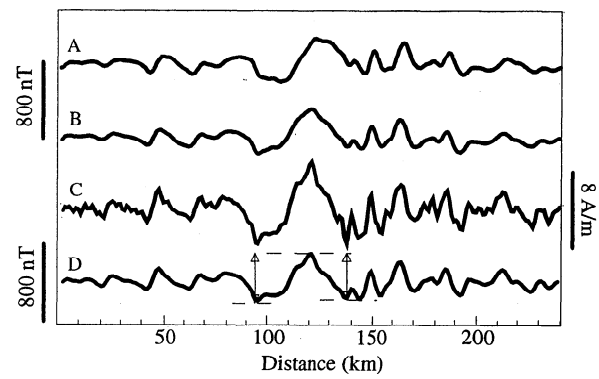

Figure 2. Example of data processing. Curve A, magnetic anomaly projected along the spreading direction and resampled at a regular interval (0.9 km); curve B, magnetic anomaly reduced to the pole using the IGRF model; curve C, equivalent magnetization computed from the magnetic anomalies by the inverse method of *Parker and Huestis* [1974] assuming a 0.5-km-thick magnetic layer following the bathymetry; curve D, magnetic anomaly computed from the equivalent magnetization by the forward method of *Parker* [1972] assuming a flat bathymetry in order to measure the peak to peak axial magnetic anomaly amplitude. Axial magnetic anomaly amplitude is the average between the peak to peak amplitude measured each side of the central anomaly (lines with arrow; see text for details).

tions complicate the rigorous determination of a significant axial magnetic signal amplitude. To minimize this problem, the equivalent magnetization is converted, by a smoothing process, to magnetic anomaly assuming a 2000-m flat topography and a 500-m-thick layer by the 2-D forward method of *Parker* [1972] (Figure 2, curve D).

Reducing magnetic anomaly profiles to correct for the effect of bathymetry through 2-D inversion with the real topography and 2-D forward computation with a flat topography is only an approximation. The equivalent magnetization determined from the original anomalies is nonunique and can be added any quantity of the annihilator, a distribution of magnetization which produces a null anomaly with the given source geometry [*Parker and Huestis*, 1974]. For a flat bathymetry (i.e., horizontal source layer), the annihilator is a constant magnetization; for extremely rough topography such as along the MAR, the annihilator may display significant variations. Converting the annihilator to magnetic anomaly assuming a flat topography results in a nonnull anomaly, which theoretically can be added in any quantity to the magnetic anomaly computed assuming a 2000-m flat topography. In practice, however, the amount of annihilator required to set the major polarity reversal to zero is added to the equivalent magnetization. Adding a reasonable quantity of the annihilator, which is in general low (two added by *Pariso et al.* [1996] at 28°N-31°30'N) or null (*Freire Luis et al.* [1994] on the Azores platform, *Pockalny et al.* [1995] between 20°and 24°N) results primarily in shifting the level of the equivalent magnetization solution and only marginally affects the relative strength of the anomalies. Our tests suggest that the error induced on magnetic anomaly amplitudes measured as described hereafter does not exceed 2%. The major advantage for converting the equivalent magnetization to anomalies at constant topography is to smooth the short-wavelength content of the magnetic signal from uncertain origin. A similar result may be achieved by applying a narrower passband filter during the inversion. We prefer the former approach in that it provides anomaly amplitudes, a quantity directly related to the magnetic anomaly measurements, instead of equivalent magnetization, a quantity which may be overinterpreted in terms of the real magnetization of rocks.

Peak to peak amplitudes are measured on both flanks of the axial magnetic anomaly and averaged to provide the uncorrected axial magnetic anomaly amplitude. A difficulty arises from the highly variable expression of the Jaramillo normal geomagnetic event, which ranges from no discernable anomaly to a marked inflection or a secondary anomaly within the slope of the axial anomaly and finally to a separate anomaly clearly distinguishable from the axial anomaly. Spreading asymmetry and/or small ridge jumps on the one hand, and the short duration of the Jaramillo normal event and the reversed polarity interval which separates it from the Brunhes period on the other hand, result in important relative variations in the width of the corresponding positively and negatively magnetized areas. We try to minimize this effect by measuring the maximum peak to peak amplitude of the axial anomaly: If a Jaramillo anomaly is clearly separated from the axial anomaly, it is not considered and the peak to peak amplitude of the axial anomaly alone is measured (Figure 2, curve D, km 140); if the Jaramillo event is characterized by an inflection or a secondary anomaly within the slope of the axial anomaly, the peak to peak amplitude of the axial anomaly including the Jaramillo event is measured (Figure 2, curve D, km 100). The uncorrected axial magnetic anomaly amplitude is corrected for the coefficient of *Schouten and McCamy* [1972]. The resulting magnetic anomaly amplitude still depends on the remanent magnetization intensity, which varies with the geomagnetic field intensity at the time of acquisition. All data are reduced to the equator assuming the remanent magnetization acquired under a geocentric axial dipole.

Another parameter which affects the shape and amplitude of the axial anomaly is the spreading rate. The rotation parameters of *Argus et al.* [1989] predict spreading rate variations along the MAR from 10 km/m.y. (half rate) at 40°N to 12.5 km/m.y. at 20°N. The effect of spreading rate on amplitude is estimated from measurement of the axial anomaly amplitude on synthetic anomaly profiles computed for various spreading rates within this range. Magnetic anomaly amplitudes are reduced to a constant spreading rate of 10 km/m.y. A summary of the different correction factors with latitude is given in Figure 3.

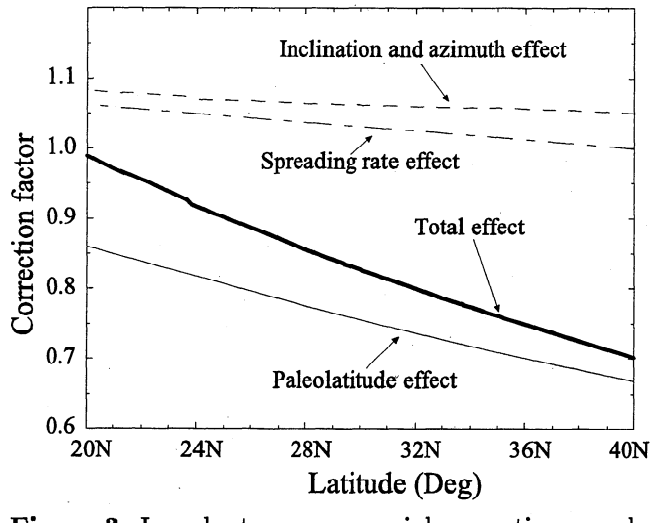

Figure 3. In order to compare axial magnetic anomaly amplitudes, several corrections must be applied to the original measurements. The correction factors along the Mid-Atlantic Ridge between 20°N and 40°N account for the C coefficient of *Schouten and McCamy* [1972] (dashed line), the effect of paleomagnetic field intensity variations with paleolatitude on remanent magnetization intensity (solid thin line; reduction to the equator), and the effect of spreading rate variations (dot-dashed line). The combination of these factors is shown by the solid thick line.

The most important potential sources of error in the axial magnetic anomaly measurements include departure from two-dimensional structure and spreading asymmetry. Departure from two-dimensional structure at the scale of 10 km along axis and at the wavelength of magnetic anomalies is relatively unimportant (< 5%), as shown by the comparison of equivalent magnetization computed along profiles (this study) and on grids at 20-24°N [*Pockalny et al.*, 1995] and at 28-31.5°N [*Pariso et al.*, 1996]. Profiles which do not present a clear axial magnetic anomaly have been rejected in the initial step of data selection. No systematic spreading asymmetry for young crust (i.e., clear Jaramillo anomaly on one side of the axial anomaly and no clear Jaramillo anomaly on the other side) has been observed at a scale larger than one ridge segment, and the possible bias induced by such spreading asymmetry would be randomly distributed along the study area and would not affect the validity of our results at a regional and local scales.

3. Axial Magnetic Anomaly Amplitudes Along the MAR

3.1. Regional Scale

Figure 4 displays axial magnetic anomaly amplitudes and other geophysical and morphological data as a function of latitude between 20°N and the Azores. The amplitudes show a monotonic succession of short-wavelength undulations whose mean value is about 450 nT, upon which two long-wavelength signals of higher amplitude are superimposed. These long-wavelength highs are better seen on the 111-km-wide running average (Figures 4d and 4e). One of them, at least 250 km wide, shows a progressive decrease of the amplitudes from 700 to 350 nT between 39°30'N and Pico FZ and most likely extends farther north [see *Freire Luis et al.*, 1994]. On the other one, 450 km wide, axial magnetic anomaly amplitudes progressively increase from 500 to 650 nT between Atlantis FZ and 28°30'N (200 km) and decrease from 650 to 450 nT between 28°30'N and 27°N (200 km).

Although they have not been previously described, both highs can also be observed from the compilation of different local magnetic anomaly studies along the MAR [*McGregor et al.*, 1977; *Schultz et al.*, 1988; *Tivey et al.*, 1993; *Freire Luis et al.*, 1994; *Pockalny et al.*, 1995; *Fujimoto et al.*, 1996; *Hussenoeder et al.*, 1996; *Pariso et al.*, 1996]. A study of (Azores platform between 37°30'N and 40°30'N) computed equivalent magnetization assuming a magnetic layer 1 km thick shows values higher than 10 A/m and up to 15 A/m [*Freire Luis et al.*, 1994]. These should be considered as minimum values as the spacing interval of grid points is only 3.3 km in the E-W direction and the data have been tapered with a cosine filter from 6.6 to 13.2 km wavelengths. A study in the vicinity of Atlantis FZ (28°N-31°30'N) [*Pariso et al.*, 1996] computed a mean equivalent magnetization assuming a magnetic layer 1 km thick of about 14 A/m; spacing interval of grid points is 2 km, and wavelengths shorter than 4 km are removed. These areas of high equivalent magnetization intensity correspond to the highs of axial magnetic anomaly amplitude displayed in Figures 4d and 4e. It is worth noting that long wavelengths (> 300 km) have been filtered out in both areas [*Freire Luis et al.*, 1994; *Pariso et al.*, 1996], and therefore the trends of increasing magnetic anomaly seen on Figures 4d and 4e may have been removed from the equivalent magnetization solutions. Farther south, magnetic anomalies have been inverted to equivalent magnetization at 26°N, on a quite small area covering two segment ends (TAG area [*McGregor et al.*, 1977; *Tivey et al.*, 1993]). Adapted to a magnetic layer thickness of 1 km, the equivalent magnetization intensities do not exceed 13 A/m and are generally close to 10 A/m, which are relatively low values compared to those of 14-18 A/m obtained at segment ends between 28°N and 31°30'N [*Pariso et al.*, 1996]. Immediately north of Kane FZ (23°30'-25°30'), equivalent magnetization computed assuming a magnetic layer 1 km thick does not exceed 10 A/m and is generally closer to 6-8 A/m [*Fujimoto et al.*, 1996; *Hussenoeder et al.*, 1996]. South of Kane FZ (20-24°N), the mean equivalent magnetization computed assuming a magnetic layer 1 km thick is about 8 A/m [*Schultz et al.*, 1988; *Pockalny et al.*, 1995]. It should be noted that the values compiled from the various studies hereabove referenced have not been corrected for the spreading rate effect, which is relatively minor (see Figure 3). It is quite likely that these values have not been corrected for the variations of magnetization intensity with paleolatitude (Figure 3), although this is not clearly stated by the authors [*McGregor et al.*, 1977; *Schultz et al.*, 1988; *Tivey et al.*, 1993; *Freire Luis et al.*, 1994; *Pockalny et al.*, 1995; *Fujimoto et al.*, 1996; *Hussenoeder et al.*, 1996; *Pariso et al.*, 1996]. However, the correction factors displayed in Figure 3 predict that the constant corrected magnetization intensity which would generate uncorrected equivalent magnetization of 8 A/m at 23°N (as observed by *Pockalny et al.* [1995]) would result in uncorrected equivalent magnetization of 9 A/m at 30°N and 10 A/m at 37°N, lower than the observed (presumably) uncorrected equivalent magnetization reported by *Pariso et al.* [1996] and *Freire Luis et al.* [1994]. Although they cover only a fraction of the investigated area, these observations are therefore in agreement with the results of our systematic study of the axial magnetic anomaly amplitude between 20°N and 40°N (Figure 4e).

In order to investigate the origin of the two long-wavelength highs of axial magnetic anomaly amplitudes, these data are compared to other morphological, geophysical, and geochemical data available along the MAR. Comparison with the along-axis bathymetry of the MAR [*Thibaud et al.*, this issue] (Figure 4g) shows that the area of high axial magnetic anomaly amplitudes between 39°30'N and Pico FZ corresponds to a shallow area (1500 m) close to the Azores hotspot known as the Azores platform. The area around Pico FZ corresponds to a steep gradient in the smoothed along-axis bathymetry (1500- 2500 m; see Figure 4g)

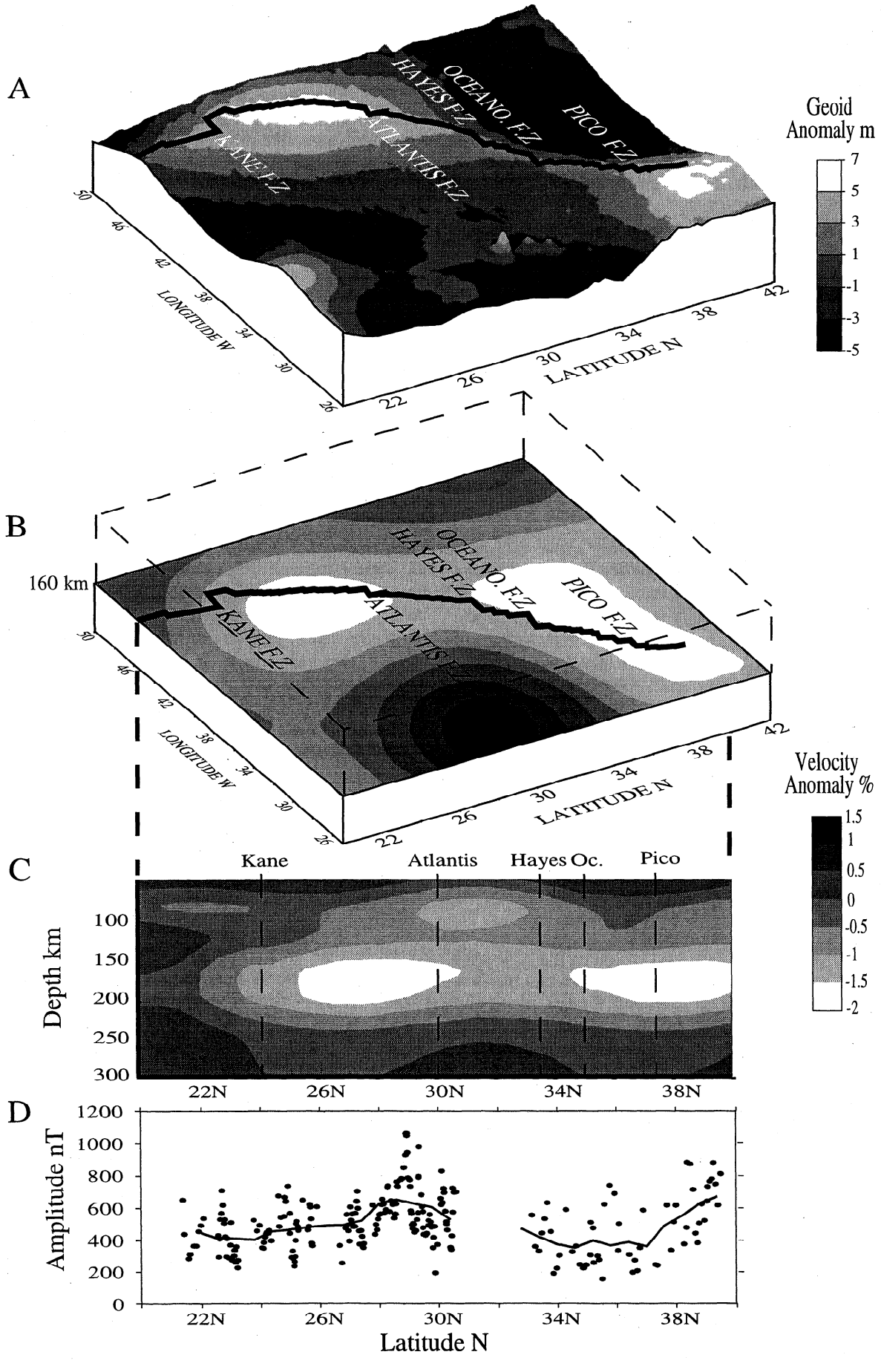
A
OCEANO. FZ
HAYES FZ
PICO FZ
KANE FZ
ATLANTIS FZ
LONGITUDE W
LATITUDE N
Geoid Anomaly m
7
5
3
1
-1
-3
-5
B
160 km
OCEANO. FZ
HAYES FZ
PICO FZ
KANE FZ
ATLANTIS FZ
LONGITUDE W
LATITUDE N
Velocity Anomaly %
1.5
1
0.5
0
-0.5
-1
-1.5
-2
C
Kane
Atlantis
Hayes Oc.
Pico
Depth km
100
150
200
250
300
22N
26N
30N
34N
38N
D
Amplitude nT
1200
1000
800
600
400
200
0
22N
26N
30N
34N
38N
Latitude N

and in the smoothed axial magnetic anomaly amplitude as well. The smoothed along-axis bathymetry progressively deepens southward from 2500 m at 37°N (Pico FZ) to 4000 m at 26°30'N [*Thibaud et al.*, this issue]. No bathymetric signature similar to that of the Azores platform is associated with the high axial magnetic anomaly amplitudes centered at 28°30'N, although a clear inflection breaks the regular slope of the smoothed bathymetry at this latitude. A closer anlysis reveals that the smoothed bathymetry signal consists in a long wavelength bathymetric trend centered on the Azores hotspot upon which intermediate wavelengths bathymetric bands of about 400 km are superimposed (Figure 4g). The long-wavelength bathymetric trend consists in an arch about 3000 km long, 1500 m high but only the southern part of it encompasses the study area. One of the intermediate-wavelengths bathymetric bands is observed at the Azores hot spot, north of Pico FZ and corresponds to a difference in bathymetric relief of 1000 m. Another one is centered at 28°30'N and shows a difference in bathymetric relief of 400 m. The location of these intermediate-wavelengths bathymetric bands correspond to that of the axial magnetic anomaly amplitude highs (Figures 4e and g).

Another bathymetric parameter of interest is the relative depth of the axial valley, which may provide indications on the fault rooting depth and therefore on the depth of the ductile-brittle mechanical transition (Figure 4h). Deeper axial valleys would be expected toward the Azores, as the spreading rate decreases. The opposite is actually observed, with axial valleys about 1500 m deep at 24°N and 800 m deep at 38°N. Again, intermediate wavelengths (about 400 km) are superimposed on a long (half) wavelength (about 3000 km) trend centered on the Azores. Intermediate wavelengths of shallower axial valleys are observed at 28°30'N and the Azores platform. In addition to shallower smoothed axial valley, these two areas present a low dispersion of the measured axial valley depth; that is, axial valleys at segment ends are particularly shallow.

The mantle Bouguer gravity anomaly (MBA) is inversely correlated to the bathymetry between 20°N and 40°N [*Thibaud et al.*, this issue] (Figure 4i). It displays a long-wavelength increase from the Azores (-200 mGal) to 26°30'N (-50 mGal), on which intermediate wavelengths of about 400 km and -20 to -40 mGal are superimposed. The lowest values of the MBA are located between 38°N and 40°N in the Azores platform [*Detrick et al.*, 1995; *Thibaud et al.*, this issue] and correspond to the area of high axial magnetic anomaly amplitudes between 39°30'N and Pico FZ. A slight inflection in the decrease of the MBA toward the Azores is associated with the high axial magnetic anomaly amplitudes centered at 28°30'N.

Intermediate-wavelength (300-3000 km) geoid data derived from satellite altimetry show positive geoid anomalies associated with the MAR. *Vogt et al.* [1984] present two significant geoid anomalies located on the Azores platform (about 6 m) and south of Atlantis FZ (about 4 m). Using the more recent data of *Cazenave et al.* [1996] and a cosine-taper filter of 2250-2750 km yields a similar result (Figures 4a and 4f). The northern positive geoid anomaly corresponds to the Azores platform, the southern one may coincide with the high of axial magnetic anomaly amplitudes centered at 28°30'N (Figures 4e and 4f). Application of a cosine-taper filter of 2750-3250 km reveals a broad positive geoid high centered on the Azores platform and extending to 24°N. The two geoid anomalies observed upon the Azores platform and south of Atlantis FZ seem therefore to be superimposed on this broader positive geoid high (Figure 4f).

Seismic velocity variations in the mantle, as revealed by seismic tomography, represent another geophysiscal data set suitable for large-scale studies. The improved resolution of recent models (about 1000 km horizontally and 100 km vertically for the *Zhang and Tanimoto* [1992] model shown in Figures 4b and 4c) allows a direct comparison with our observations along the MAR. Two large anomalies of low seismic velocity are clearly asso-

Figure 4. (opposite) Various morphological and geophysical data along the Mid-Atlantic Ridge between 20°N and 40°N. (a) Intermediate-wavelength geoid anomaly (low-pass cosine taper filter of 2250-2750 km, data from *Cazenave et al.* [1996]); the Mid-Atlantic Ridge axis is shown by a thick line; (b) seismic velocity anomaly model on a horizontal section at 160 km depth [from *Zhang and Tanimoto,* 1992]; (c) seismic velocity anomaly model on a vertical section along the Mid-Atlantic Ridge axis [from *Zhang and Tanimoto,* 1992]; (d) axial magnetic anomaly amplitude measurements (dots) and 111-km-wide running average (thick line); for amplitude measurement location, refer to Figure 1; (e) smoothed axial magnetic anomaly amplitude (111-km-wide running average; thick line) and equivalent magnetization of the axial magnetic anomaly compiled from published magnetic studies along the Mid-Atlantic Ridge between 20°N and 40°N (see references in text); the dashed line shows the (presumably) uncorrected equivalent magnetization, and the solid line shows the equivalent magnetization corrected with the correction factors displayed in Figure 3; (f) along-axis intermediate wavelength geoid anomaly (low-pass cosine taper filter of 2250-2750 km, solid dots; of 2750-3250 km, open dots; data from *Cazenave et al.* [1996]); (g) along-axis bathymetry of the axial valley (thin line from *Thibaud et al.* [this issue]) and 200-km-wide running average (thick line); (h) depth of the axial valley (i.e., amplitude of the relief from valley to crests, thin line) and 200-km-wide running average (thick line); (i) along-axis mantle Bouguer gravity anomaly (thin line) from *Thibaud et al.* [this issue]) and 200-km-wide running average (thick line). All of these data present two intermediate-wavelength signals located on the Azores platform and south of Atlantis FZ.

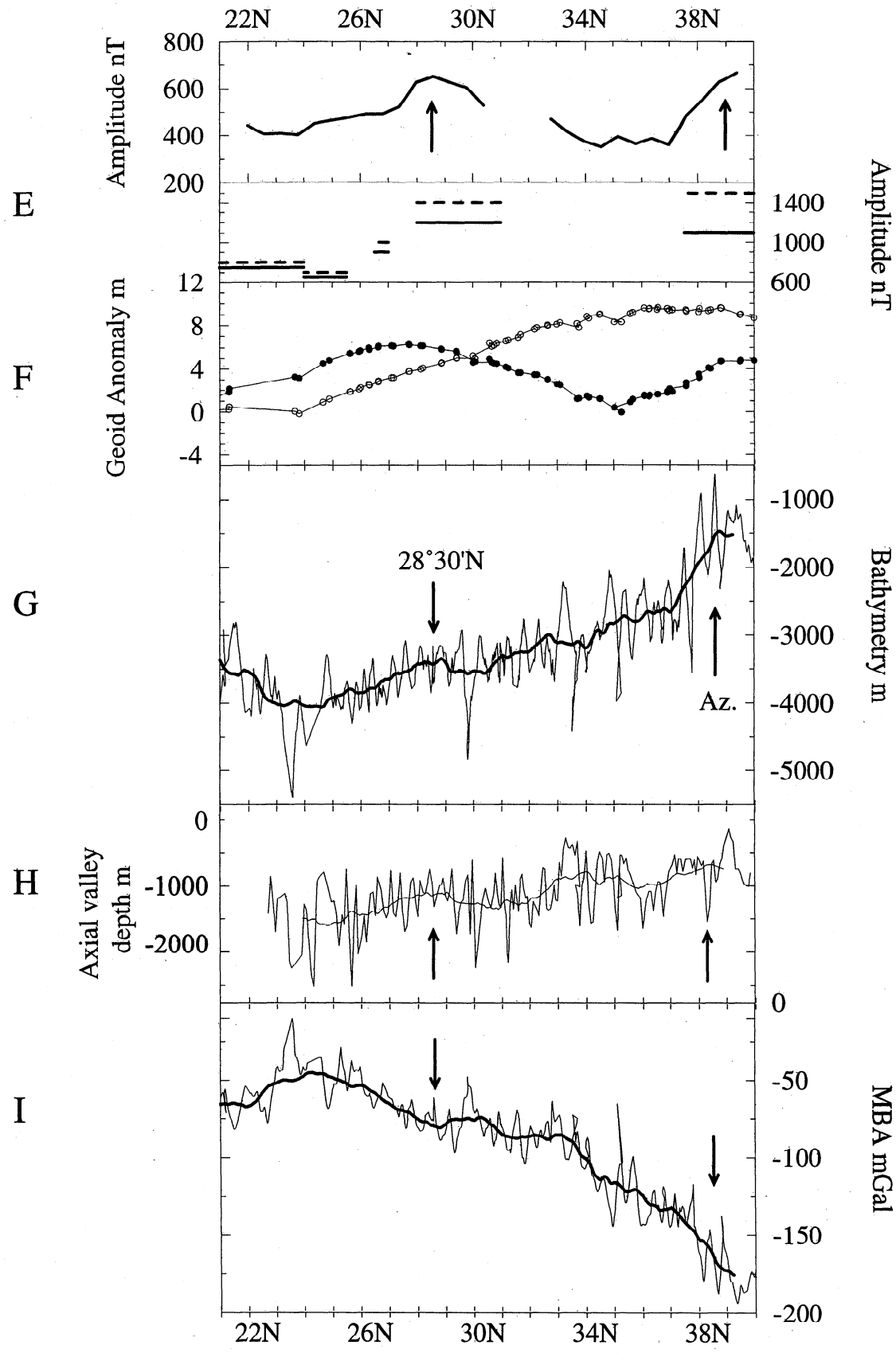

Figure 4. (continued)

ciated to the MAR (Figure 4b) and extend from about 100 to 200 km deep (Figure 4c). One of these anomalies has been related to the Azores hotspot [*Zhang and Tanimoto,* 1992]; the other one is located south of Atlantis FZ and may correspond to the high of axial magnetic anomaly amplitudes centered at 28°30'N. It should be noted, however, that despite the improved resolution of this model, the 2600-km-long section of our magnetic study corresponds to only three points in the seismic data.

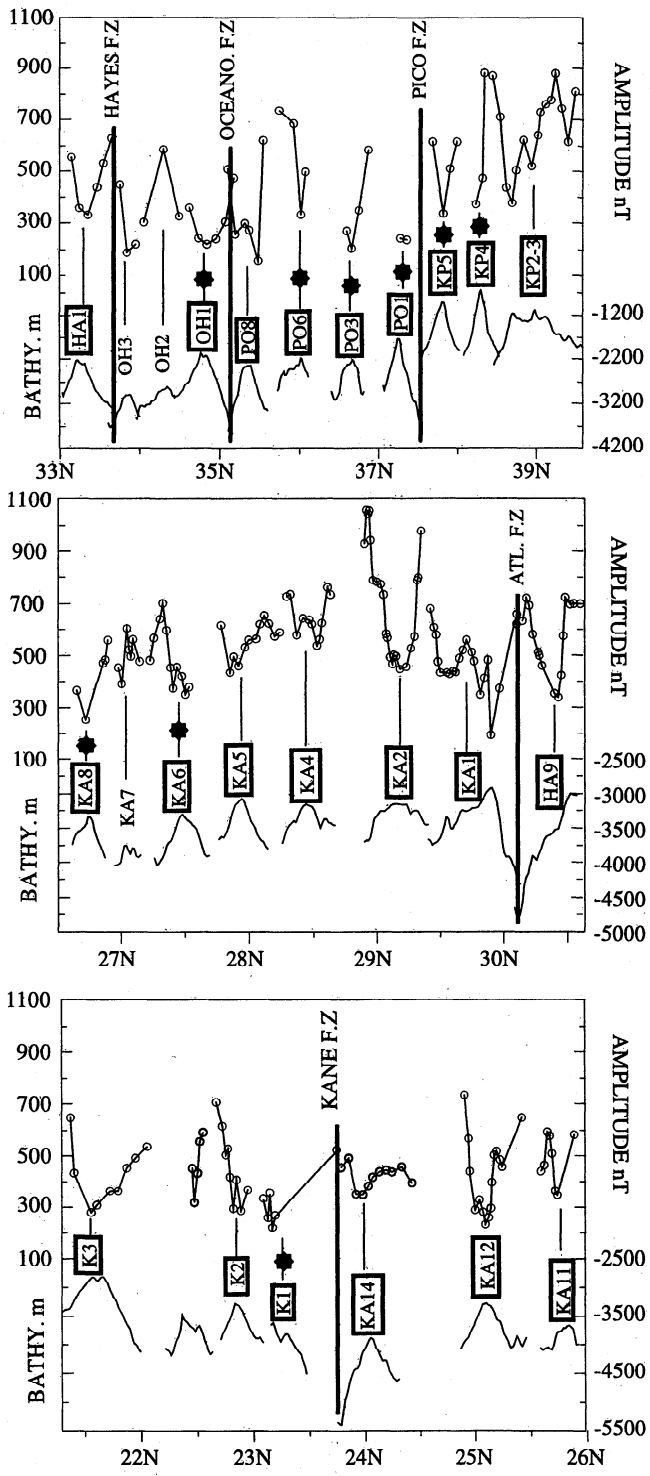

Among the numerous major, trace, and isotopic elements which have been studied along the MAR [e.g., *Melson and O'Hearn,* 1979; *Morel and Hékinian,* 1980; *Schilling et al.,* 1983; *Schilling,* 1986; *Klein and Langmuir,* 1989; *Dosso et al.,* 1993], the variations of iron and titanium oxide contents are of prime importance for comparison with axial magnetic anomaly amplitudes. Various parameters are derived from the direct measurement of FeO*: $Fe_{8.0}$ is reduced to a constant 8.0 wt % MgO to correct for shallow-level fractionation [*Klein and Langmuir,* 1987], $Fe^G_{8.0}$ is furthermore corrected for the "local trend" [*Klein and Langmuir,* 1989]. *Klein and Langmuir* [1989, Figure 10] present both $Fe_{8.0}$ and $Fe^G_{8.0}$ along the MAR. Although measurements are by far much denser in the vicinities of the Azores and in the MARK area south of Kane FZ, $Fe_{8.0}$ shows no significant trend between 20°N and 40°N, whereas $Fe^G_{8.0}$ presents a positive slope from Kane FZ toward the Azores. It should be noted that in both cases, the dispersion of measured values increases toward the Azores. High Ti contents are also found in basalts over the Azores [*Schilling et al.,* 1983].

3.2. Segment Scale

Figure 5 shows the axial magnetic anomaly amplitude and associated bathymetry along the MAR axis. Segments are numbered in accordance to *Detrick et al.* [1995] and *Thibaud et al.* [this issue]. All segments (except segment OH2 at 34°20'N) present an inverse relationship between depth and axial magnetic anomaly amplitude. The magnetic anomaly amplitude is about twice as high at segment ends than at segment center. This result generalizes those of *Pockalny et al.* [1995], *Hussenoeder et al.* [1996], and *Pariso et al.* [1996] for MAR segments located between 20°N and 24°N, 24°N and 24°40'N, and 28°N and 31°N, respectively. Similar observations have also been made on several segments in the South Atlantic [*Grindlay et al.,* 1992; *Weiland and Macdonald,* 1993; *Weiland et al.,* 1996] and in the Pacific [*Detrick and Lynn,* 1975; *Sempéré,* 1991; *Carbotte and Macdonald,* 1992; *Tivey,* 1994].

Axial magnetic anomaly amplitudes within each segment exhibit a large spectrum of along-axis variations,

Figure 5. Left axis shows location of the surface magnetic anomaly profiles (thin lines) between (bottom) 21-31°N and (top) 33-40°N. Right axis shows (top) axial magnetic anomaly amplitude and (bottom) bathymetry [from *Thibaud et al.,* this issue] along the Mid-Atlantic Ridge axis between 21-26°N (bottom), 26-31°N (middle), and 33-40°N (top). Fracture zones are indicated by thick vertical lines, segment centers by thin vertical lines. Except for segment OH2 at 34°20'N, axial magnetic anomaly amplitude is systematically higher at segment ends than at centers. Segment names within a box indicate segments taken into account in the analysis of amplitude parameters versus ΔMBA. Stars indicate segments where data coverage is poor and considered less reliable in the analysis of amplitude parameters versus ΔMBA (open dots in Figures 6b, 6c, and 6d).

from a simple bowl shape (e.g., segments OH1 and KP5, see Figure 5) to more complex undulations presenting several lows (e.g., segments KP2-3 and KA1). Segment center is marked either by the lower part of a depression (e.g., segment HA1) or by a local, low-amplitude, and short-wavelength high within a longer-wavelength, higher-amplitude low (e.g., segments PO8 and KA4). Amplitudes toward the segment ends display symmetrical (e.g., segments KP5 and OH1) or asymmetrical (e.g., segments PO6, KA14, and K3) variations. Slightly decreasing (e.g., segment KA5 and KA14) or constant (e.g., segment HA9) amplitudes are locally observed at segment ends, in the vicinity of the discontinuities. Where the data coverage is dense enough, an inverse correlation between axial magnetic anomaly amplitude and along-axis bathymetry is sometimes observed at the most detailed scale (e.g., segment KA12).

ΔMBA is defined as the maximum range of the MBA within a segment [see *Lin et al.*, 1990]. This parameter is interpreted in terms of along-axis variations of crustal thickness and/or density of the crust and/or the uppermost mantle, all of them possibly reflecting thermal variations within the segment. ΔMBA seems also sensitive to a geometrical effect: large ΔMBA correspond to long segments and conversely low ΔMBA to short segments [*Lin et al.*, 1990; *Detrick et al.*, 1995; *Thibaud et al.*, this issue]. However, *Thibaud et al.* [this issue] show that morphotectonic parameters also vary in a consistent way with ΔMBA: narrow and shallow axial valleys at segment centers are associated with large ΔMBA, wide and deep axial valleys at segment centers with low ΔMBA. This suggests that ΔMBA and therefore the segment length indeed reflect the thermal state of a segment: a high ΔMBA (a long segment) means a hotter and magmatically active segment with shallow and closely spaced along-axis isotherms, whereas a low ΔMBA (a short segment) means a cooler and magmatically less active segment with deep and widely spaced isotherms. This is consistent with the observed propagation of segments associated with robust magmatic activity at the expense of the neighboring, less magmatically active segments.

Previous studies of axial magnetic anomaly amplitude (or of equivalent magnetization) focused on only one or very few segments [e.g., *Tivey and Johnson*, 1987; *Grindlay et al.*, 1992; *Tivey et al.*, 1993; *Weiland and Macdonald*, 1993; *Pockalny et al.*, 1995; *Hussenoeder et al.* 1996; *Pariso et al.*, 1996; *Weiland et al.*, 1996]. Here we take advantage of the large number of segments within our study area to analyze the axial magnetic anomaly amplitude along the MAR by comparison with ΔMBA. Four parameters reflecting axial magnetic anomaly amplitude variations within and among segments are considered. Similar to ΔMBA, we define ΔA as the range of along-axis magnetic anomaly amplitude within a segment, i.e., the difference measured at midsegment of the linear interpolation between highest amplitudes (at segment ends) and the amplitude observed at segment center. For segments which present amplitude measurement on only one half (e.g., KP4), ΔA is approximated by the difference between the amplitudes measured at segment center and at the available segment end. ΔA is a relative parameter which reflects the variations of axial magnetic anomaly amplitude among segments. We define A_c as the amplitude at segment center, i.e., measured at (or in a close vicinity of) the bathymetric high. A_c generally corresponds to the lowest axial magnetic anomaly amplitude observed in the segment; it is only close to the lowest amplitude for segments where a local, low-amplitude and short-wavelength high is present (e.g., segment KA4). Similarly, we define A_e as the amplitude at segment ends, i.e., the mean of the high amplitudes measured at (or in a close vicinity of) the segment ends. Both A_c and A_e are local parameters which cannot be measured on all segments. A_m is the mean of A_c and A_e and is close to the median of the axial magnetic anomaly amplitude. In this respect, it may be more representative of the axial magnetic anomaly amplitude at the scale of the segment; for instance, segments KA2 and KA5 display similar A_c but very different ΔA which result in lower A_m for segment KA5 than for segment KA2, in agreement with the smoothed axial magnetic anomaly amplitude obtained by running averages (Figures 4d and 4e). The four parameters contain redundant information and can be deduced from the combination of two of them. For instance, $A_e = A_c + \Delta A$ and $A_m = A_c + \Delta A / 2$. Segments OH2, OH3, and KA7 have not been considered for further analysis. Segment OH2 presents only three measurements with higher amplitude at the segment center than at segment ends; more data are required to confirm these anomalous observations with respect to the other segments. Segment OH3 presents only three amplitude measurements, and none are located upon the bathymetric high. Segment KA7 is very short (28 km) and does not present a well-marked bathymetric high so the segment center is difficult to identify. Segment PO1 displays only two measurements at the segment center and is only considered for determination of A_c.

Figure 6a represents ΔA versus ΔMBA. These two parameters show a relatively good correlation (R = 0.86) aside for segments HA9, KA2, and OH1 which are not included in the correlation. Segments HA9 and KA2 are affected by the regional high of the axial magnetic anomaly amplitudes centered at 28°30'N, which is associated to relatively low variations of both the MBA and ΔMBA with regard to those observed at the Azores platform amplitude high (see regional scale). Segment KA2, located at 29°N close to the center of this area, shows higher ΔA than expected because of very high amplitudes (about 1000 nT) at the segment ends. In addition, hydrothermal activity at the Broken Spur site [*Murton et al.*, 1994] may lower the relative amplitude at the center of the segment. Conversely, the lack of data at the southern end of segment OH1 results in a likely underestimated ΔA for this segment. For all other segments, low ΔMBA are associated with low ΔA and high ΔMBA with high ΔA. ΔA present a lower variability for colder segments (generally low ΔMBA,

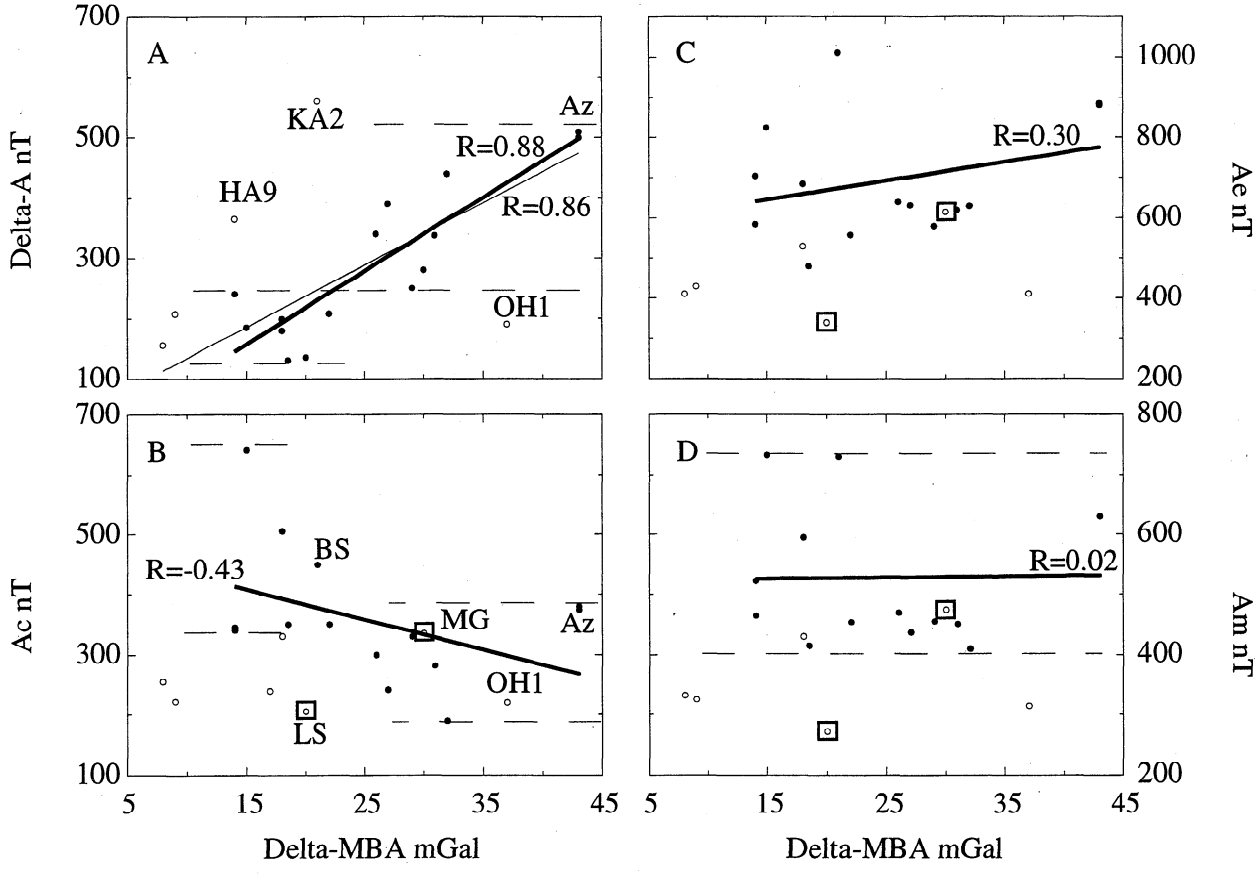

Figure 6. (a) Range of axial magnetic anomaly amplitude (ΔA) versus range of mantle Bouguer gravity anomaly (ΔMBA). Except for segments KA2, HA9, and OH1, these two parameters present a clear correlation (thin line, R=0.86 and thick line, R=0.88 if segments associated with a ΔMBA less than 10 mGal are rejected) AZ; segments associated with the Azores platform. (b) Amplitude at segment center (A_c) versus ΔMBA. Open dots indicate segments with a poor data coverage (see stars on Figure 5) and open squares indicate segments associated with hydrothermal activity (LS; Lucky Strike; MG; Menez Gween; BS; Broken Spur). The thin dashed lines schematize the data repartition for colder (10-20 mGal) and hotter (more than 20 mGal) segments. (c) Amplitude at segment ends (A_e) versus ΔMBA. Same symbols as in Figure 6b. (d) Median amplitude (A_m) versus ΔMBA. Same symbols as in B. These relations suggest that amplitude variations within segments are strongly related to their thermal state, reflected by ΔMBA. Hotter segments (large ΔMBA) present relatively low amplitude at segment center and high ΔA, whereas colder segments (low ΔMBA) present variable and relatively high amplitude at segment center and low ΔA.

see above), with a dispersion of 90 nT, than for hotter segments (high ΔMBA), with a scatter of more than 250 nT (more than 200 nT if segments KP2-3 and KP4 located upon the Azores platform are not considered).

Figure 6b, 6c, and 6d represent A_c (axial magnetic anomaly amplitude at segment centers), A_e (axial magnetic anomaly amplitude at segment ends), and A_m (median axial magnetic anomaly amplitude) versus ΔMBA. Segments with a poor data coverage, most of them located north of 33°N, are shown with open dots (KP5, P01, P03, OH1, KA8, and K1). These segments either include less than four measurements or do not include measurement at segment center or at one of the segment ends. Parameters A_c, A_e, A_m and ΔA are less reliable for these segments. Additionally, it should be noted that segments KA8 and K1 are shorter than 40 km and present ΔMBA lower than 10 mGal and low A_c, A_e, A_m and ΔA as well. It is likely that these low values result in part from the geometric effect. As ΔMBA have been obtained from satellite-derived gravity data [*Thibaud et al.*, this issue] and the resolution of these data is about 20 km at best [*Sandwell and Smith*, 1997], we consider Δ MBA for the segments shorter than 40 km as less reliable.

No simple relationship is observed between A_c, A_e, A_m and ΔMBA (Figures 6b, 6c, and 6d). Segments longer than 40 km, i.e., associated with a ΔMBA higher than 10 mGal, can be separated in two groups, segments with ΔMBA ranging from 10 to about 20 mGal (hereafter designed as "colder segment," see discussion in section 3.2) and segments with ΔMBA higher than 20 mGal ("hotter segments"). A_c is relatively high and scattered for colder segments (350-650 nT including only reliable data) and shows lower values and disper-

sion (200-400 nT) for hotter segments. Conversely, A_e present relatively low values and dispersion for colder segments (450-700 nT) and a higher dispersion (550-1100 nT) for hotter segments; the latter results from the high amplitude at segment ends for segments KA2 and KP2-3, centered at 29°N and on the Azores platform, respectively (see regional scale). A_m present mixed patterns, with values ranging between 400 and 750 nT for both the colder and hotter segments.

Parameters like A_c, A_e and to a lesser extent A_m are local parameters that do not take into account the along-axis variations of the axial magnetic anomaly amplitude within each segment. We attempt to consider the whole set of available amplitude measurements by normalizing the distance along each half segment (from segment center to one segment end) by the total length of the half segment and superimposing measurements of the axial magnetic anomaly amplitude for all half-segments on the same plot. The resulting plot is mirrored for visual clarity (Figure 7a). Despite the large dispersion, amplitude at segment ends is clearly higher than at segment center. The dispersion is larger at segment ends (400-900 nT) than at segment center (200-600 nT) and is slightly attenuated if segments associated with the two long-wavelength magnetic highs centered at 39°30'N and at 28°30'N (see above, regional scale) are discarded (Figure 7b). In agreement with previous observations, segments are separated in two groups with respect to their ΔMBA (Figures 7c and 7d). Segments with ΔMBA higher than 25 mGal

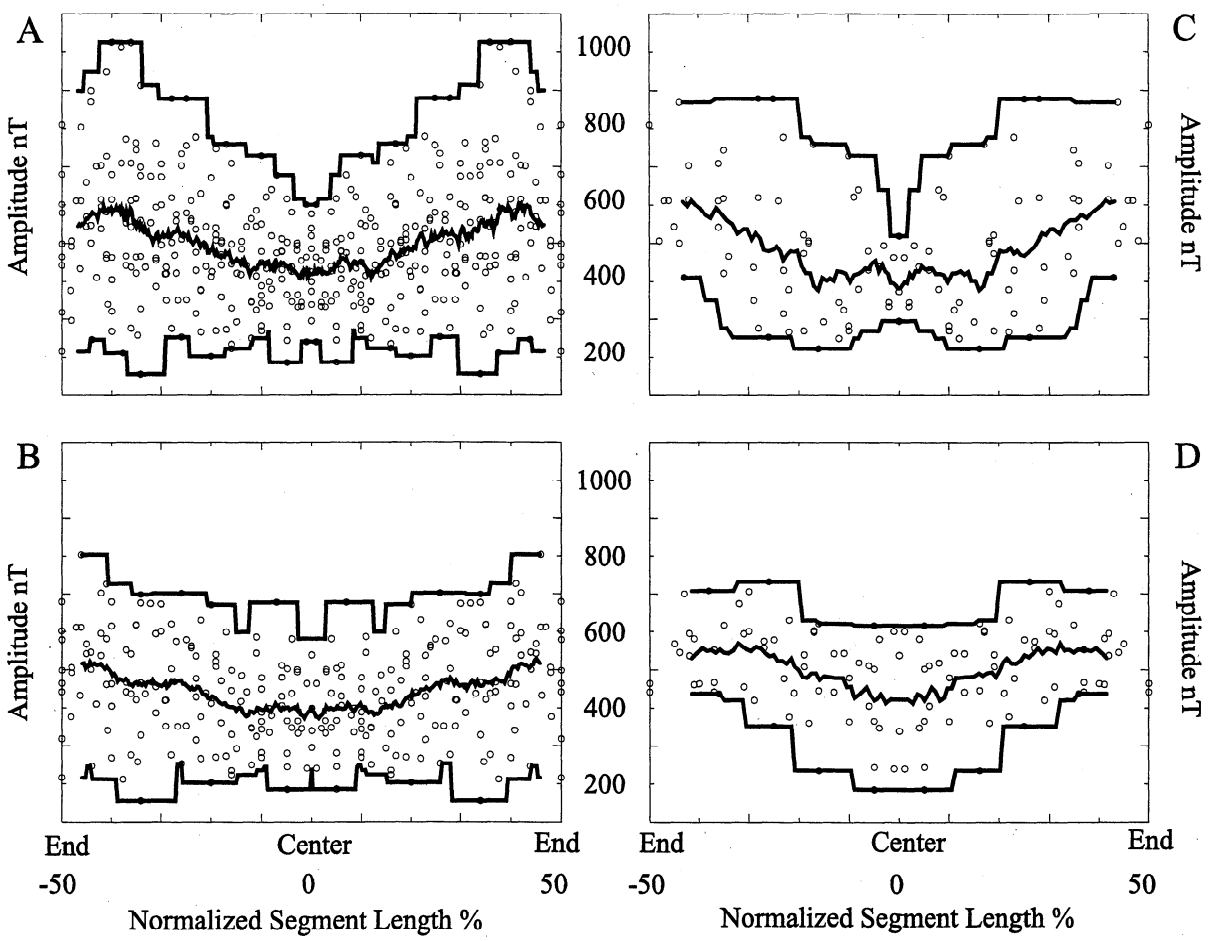

Figure 7. Axial magnetic anomaly amplitudes versus distances normalized to segment half length (0 is the segment center, 50 is the segment end). The diagrams are mirrored (from -50 to 0) to display full segment variations. (a) All segments are considered. Axial magnetic anomaly amplitude increases toward segment ends, and dispersion of the measurements increases accordingly. Dispersion is quite important both at segment centers and ends. Thick lines are computed by running averages (maximum, median, and minimum). (b) All segments are considered, except those affected by the high of axial magnetic anomaly amplitudes at regional scale. Dispersion is slightly reduced, especially at segment ends. Thick lines are computed by running averages. (c) Segments with ΔMBA high than 25 mGal are considered. Axial magnetic anomaly amplitudes are grouped at segment centers and more dispersed at segment ends. Thick lines are computed by running averages. (d) Segments with ΔMBA lower than 18 mGal are considered. Axial magnetic anomaly amplitudes are scattered at segment centers and grouped at segment ends. Thick lines are computed by running averages.

("hotter segments," see discussion in section 3.2: KP2-3, KP4, KP5, PO8, OH1, KA12; Figure 7c) display grouped amplitudes at segment center (300-550 nT) and scattered amplitudes at middistance between center and ends (250-900 nT) and at segment ends (400-900 nT). Conversely, segments with ΔMBA lower than 18 mGal ("colder segments": HA9, KA4, KA5, KA6, KA8, KA11; Figure 7d) present scattered amplitudes at segment center (150-650 nT) and a lower dispersion at middistance between center and ends and at segment ends (400-750 nT).

The correlation between ΔA and ΔMBA and the emergence of two classes of segments depending on ΔMBA show that hotter and magmatically active segments correspond to a large range of axial magnetic anomaly amplitudes within the segment, relatively low and uniform amplitudes at segment centers, and scattered amplitudes at segment ends, whereas colder and less magmatically active segments correspond to a narrower range of amplitude, scattered amplitudes at segment centers, and uniform amplitudes at segment ends.

4. Discussion

4.1. Regional Scale: The Azores Hotspot and More?

4.1.1. Azores long-wavelength amplitude high. As shown in section 3.1, the Azores area is characterized by a long-wavelength high of the axial magnetic anomaly amplitudes. The Azores hotspot is also associated with a strong signature on the bathymetry and the MBA, which extend southward as far as about 26°N (Figure 4). To explain the large gravity low beneath the Azores platform, variations of the crustal thickness and/or the underlying mantle density are required. The crust is estimated to be 8-9 km thick at the Azores platform [*Detrick et al.*, 1995]. Although studies in others portions of the MAR and elsewhere show that along-axis thickness variations of the seismically defined crustal layers within segments occurs principally in layer 3 [e.g., *Tolstoy et al.*, 1993; *Mutter and Mutter*, 1993], it is most likely that the extrusive basaltic layer thickness varies as a function of the magmatic activity in the segment. The nature of the seismic boundary between layers 2 and 3, often confused with the petrological boundary between the basaltic and gabbroic layers, instead corresponds to a [*Detrick et al.*, 1994, p. 289] "transition in physical properties [...] controlled by many factors including bulk porosity, fracture geometry and crustal alteration, as well as by igneous petrology," as suggested by the comparison of seismic and drilling results around Deep Sea Drilling Project (DSDP) Hole 504B. The variation of magmatic activity among and within segments and the outcrops of deeper crustal and mantle rocks along the less magmatically active segments and in the vicinity of most of the segment ends support variations of the extrusive basaltic layer thickness with magmatic activity (see *Lagabrielle et al.* [1998] for a review along the MAR]. Such variations are also widely observed on ophiolitic sections created at slow spreading centers [*Lagabrielle and Cannat*, 1990]. The high axial magnetic anomaly amplitudes observed on the Azores platform may therefore be interpreted as reflecting thick extrusive basalts, hence a thick magnetic source layer. Assuming uniform magnetic properties within the extrusive basalts, variation from a normal 500-m-thick extrusive layer to a 800-m-thick one would be sufficient to explain the observed high amplitudes. Although deeper sources may also contribute to marine magnetic anomalies at slow and intermediate spreading centers [e.g., *Pariso and Johnson*, 1993; *Dyment and Arkani-Hamed*, 1995; *Dyment et al.*, 1997], the major magnetic source layer is constituted by the upper extrusive basalts. This is especially true for the axial magnetic anomaly, because cooling of deeper potential sources below the Curie isotherm and alteration of the highly magnetized titanomagnetites in the extrusive basalts may not be completed.

Another, complementary explanation of these high axial magnetic anomaly amplitudes may be found in the high iron and titanium content as well [*Melson and O'Hearn*, 1979; *Morel and Hekinian*, 1980; *Sigurdsson*, 1981; *Klein and Langmuir*, 1989]. Geochemically, a distinct magmatic source is associated with the Azores hotspot, as suggested by the distribution of major, trace, and isotopic elements along the MAR [*Melson and O'Hearn*, 1979; *Morel and Hékinian*, 1980; *Schilling et al.*, 1983; *Schilling*, 1986; *Klein and Langmuir*, 1989; *Dosso et al.*, 1993]. The intermediate-wavelength geoid and bathymetric highs are consistent with a thermal anomaly below the Azores. Conversely, the deep low seismic velocity anomaly underlying the Azores area as revealed by seismic tomography can be interpreted in terms of high temperatures, chemical heterogeneities, or the presence of fluids. However, it is generally estimated that chemical heterogeneities have minor effects on lateral velocity variations [*Su and Dziewonski*, 1991; *Ranalli*, 1996]. High mantle temperatures and/or the presence of fluids generate a greater amount of ascending melt and therefore a thicker magmatic crust; melt extracted at greater depth (pressure) presents a high content in iron and results in Fe-enriched erupted lavas [*Klein and Langmuir*, 1989; *Bonatti*, 1990]. Although there is no simple and direct relationship between them [e.g., *Sempéré*, 1991], it is most likely that high Fe-Ti contents increase the amount of magnetic minerals and the axial magnetic anomaly amplitudes in this portion of the MAR, in agreement with the magnetic telechemistry hypothesis [*Vogt and Johnson*, 1973].

Therefore the various correlations observed between the long-wavelength signal of high axial magnetic anomaly amplitudes between 39°30'N and Pico FZ and other morphological, geophysical, and geochemical data set along the MAR support a thick and/or Fe-Ti-enriched magnetic source layer on the Azores platform.

4.1.2. The 28°30'N long-wavelength amplitude high. The magnetic high centered at 28°30'N is associated with intermediate-wavelength (400 km) signatures in the bathymetry of the MAR axis, the depth of the axial valley, and the MBA. These signatures are

about half those associated, at the same wavelength, with the Azores platform and may also reflect the presence of a thermal anomaly. The shallow depth of the axial valley, consistently observed at segment centers and ends around 28°30'N, suggest a shallower brittle-ductile transition, in agreement with such a perturbation. In addition, the 28°30'N area is marked by a geoid high in the wavelengths lower than 2500 km and by a large anomaly of low seismic velocity. Both may reflect sublithospheric processes responsible for the high axial magnetic anomaly amplitudes in this area. Again, higher mantle temperatures and/or the presence of fluids generate a greater amount of ascending melt and therefore a thicker magmatic crust (800 m); melt extracted at greater depth (and pressure) presents a high content in iron and results in Fe-enriched erupted lavas [*Klein and Langmuir,* 1989; *Bonatti,* 1990]. The presence or absence of iron and titanium-enriched basalts in the vicinity of 28°30'N cannot be convincingly constrained by the sparse geochemical data available along this part of the MAR.

Morphological and geophysical evidence for thermal anomalies beneath the Azores and at 28°30'N is indeed qualitatively similar at intermediate wavelength (400 km), although it is most likely that the thermal anomaly at 28°30'N is weaker than that of the Azores. The major difference is at long wavelength: the Azores lies at the center of a large, 3000-km-wide zone of influence which may reflect the deeper expression of the Azores hotspot. No such long-wavelength expression is associated to the 28°30'N area. The 28°30'N thermal anomaly may be a secondary branch of the Azores hotspot, which would individualize from the main plume at relatively shallow depth, possibly in relation with the presence of the MAR; it may also be independent from the Azores hotspot and correspond to the weakened remnant of a hotspot responsible for the formation of the New England Seamounts, which presently lies at about 27°N, 43°E [*O'Connors and Duncan,* 1990].

4.2. Segment Scale: Toward a Model for Axial Magnetic Amplitude Variations?

The observed variations of axial magnetic anomaly amplitude suggest that the structure and magnetic properties of the magnetic source layer vary in a consistent way along most segments of the MAR in the study area. Four major processes, which all depend on the thermal structure of the ridge segment, have been proposed to explain the variations of magnetic anomaly amplitude within ridge segments: higher degree of alteration due to more pervasive faulting and hydrothermal fluid circulation at segment centers [*Tivey and Johnson,* 1987; *Wooldridge et al.,* 1992], deepening Curie isotherm from segment center to ends [*Grindlay et al.,* 1992; *Tivey et al.,* 1993; *Pariso et al.,* 1996], serpentinization of outcropping peridotites at segment ends [*Pockalny et al.,* 1995; *Pariso et al.,* 1996], increasing fractionation and iron content from segment center to ends [*Weiland and Macdonald,* 1993; *Weiland et al.,* 1996]. The new observations derived from our analysis of a large number of segments indicate that the thermal state of the segment strongly influences ΔA, the range of axial magnetic anomaly amplitudes within the segment: along-axis amplitudes variations among segments are stronger in segments characterized by a large ΔMBA and a robust volcanic activity than in segments presenting a low ΔMBA and a weak magmatic activity. Moreover, hotter and magmatically active segments display relatively low and uniform amplitudes at segment centers and scattered amplitudes at segment ends, whereas colder and less magmatically active segments show scattered amplitudes at segment centers and uniform amplitudes at segment ends. In the light of these inferences, we examine the various proposed processes and attempt to model the along-axis axial magnetic anomaly amplitude variations corresponding to each of these processes for different thermal state of the segment. At this stage, this modeling effort is more conceptual than quantitative and rests on the following simplistic, although most generally verified [see *Thibaud et al.,* this iussue], assumptions: both the length of the segment and ΔMBA increase with the magmatic activity of the segment and the temperature at the center of the segment. Most thermal models suggest that temperatures at the center of segments associated with large ΔMBA are higher than at the center of less magmatically active segments, whereas temperatures at the ends of both types of segments are quite similar [e.g., *Detrick et al.,* 1995]. Such statement is supported by the observation of ridge propagation away from hotter and magmatically active segments at the expense of the neighboring colder segments [e.g., *Thibaud et al.,* this issue]: such propagation would roughly tend to restore uniform along-axis thermal gradient and keep constant the temperature at segment ends.

4.2.1. Low-temperature alteration through faulting and hydrothermal circulation. Alteration of extrusive basalts through faulting and hydrothermal circulation reduces magnetization of oceanic basalts and the amplitude of marine magnetic anomalies by the transformation of titanomagnetite to titanomaghemite [e.g., *Rona,* 1978; *Wooldridge et al.,* 1990]. Such a process has been proposed to explain the decay of rock magnetization and of magnetic anomaly amplitude with age [e.g., *Dunlop and Hale,* 1977; *Macdonald,* 1977; *Bleil and Petersen,* 1983; *Geiss et al.,* 1989; *Wittpenn et al.,* 1989; *Wooldridge et al.,* 1990; *Sayanagi and Tamaki,* 1992; *Furuta,* 1993; *Johnson and Pariso,* 1993; *Gee and Kent,* 1994]. To account for the variations of axial magnetic anomaly amplitude within segments, alteration should be more efficient at segment center than at segment ends. The major difficulty to relate alteration and the amplitude variations is the poor knowledge of the systematics of faulting and hydrothermal circulation along a ridge segment. Segment PO1, which includes hydrothermal site Lucky Strike [*Langmuir et al.,* 1993], exhibits very low amplitude at segment center A_c, in agreement with the notable reduction of surface and deep-tow magnetic measurements observed at the TAG hydrothermal site [*Tivey et al.,* 1996]. Conversely,

the amplitude at the center of segment KP5, which includes hydrothermal site Menez Gwen [*Fouquet et al.*, 1994], is similar to that of the other segments investigated, and the amplitude at the center of segment KA2, which includes hydrothermal site Broken Spur [*Murton et al.*, 1994], is relatively high (Figure 6b). The pervasive hydrothermal activity observed at these sites seems therefore to produce local reduction of the anomaly amplitude, insufficient to explain the systematic variations of axial magnetic anomaly amplitude. Alteration has also been inferred to explain the observation, on deep-tow magnetic measurements, of low magnetic anomaly amplitude and low equivalent magnetization on the axial valley walls at 24°N-24°40'N [*Hussenoeder et al.*, 1996]. The reduction in amplitude of the anomaly measured at the surface seems, however, limited to the vicinity of the valley walls, affected by faults which permit easy seawater circulation. If it modifies the shape of the axial magnetic anomaly, it does not significantly affect the peak to peak amplitude measurement of the axial magnetic anomaly. Hence we do not consider alteration as a plausible cause to explain the systematic amplitude variations observed within and among the segments investigated. Instead, we consider alteration as a complementary process which may locally decrease significantly the magnetization and therefore the amplitude of the anomaly.

4.2.2. Variable Curie isotherm depth. As suggested in section 4.1, significant variations of the magnetic layer thickness related to sublithospheric thermal anomaly and on magma production may partially account for the two areas of high axial magnetic anomaly amplitudes. At segment scale, segment centers are the magmatic centers and should have thicker extrusive and thus higher magnetic amplitude. The opposite is actually observed as segment centers are associated with low amplitudes. This apparent paradox may result from the depth to the Curie isotherm which is modified by moderate thermal variations [*Grindlay et al.*, 1992; *Wooldridge et al.*, 1992] and may therefore have a strong influence on the thickness of the magnetized layer, hence on the axial magnetic anomaly amplitudes. Depth to the Curie isotherm varies with the thermal structure of the segment and may explain variations of the axial magnetic anomaly amplitude within segment; it also depends on the thermal state of the segment and may explain variations of amplitude among segments. Under the assumption that the thermal state of the segments is principally controlled by thermal variations at segments centers and that the temperatures at segment

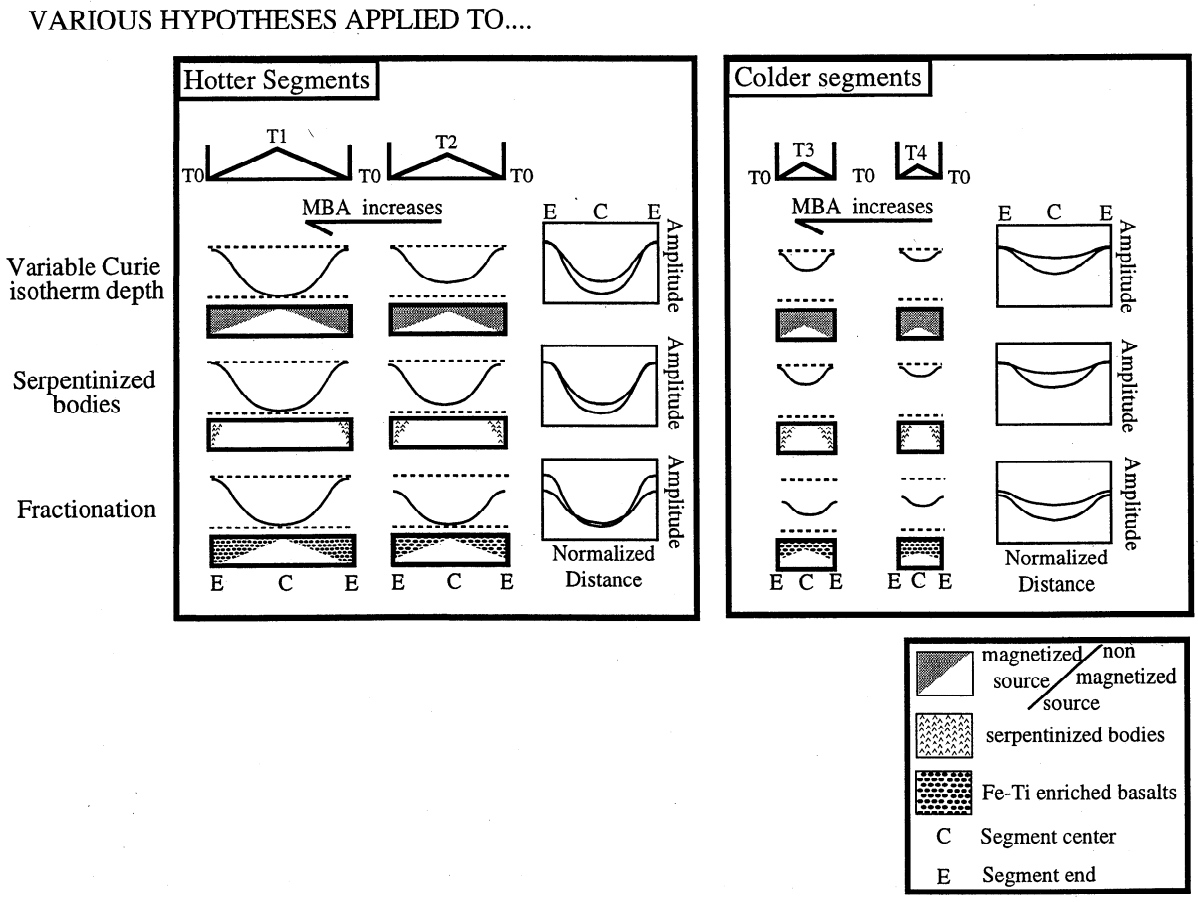

Figure 8. Schematic sketches presenting the along-axis variations of axial magnetic anomaly amplitudes expected for three possible processes at (left) hotter and (right) colder segments. The along-axis amplitude variations predicted for each segments are normalized to the segment length to be compared with Figure 7 (see text for discussion).

ends are almost uniform (see section 3.2), this process would predict a rather uniform magnetic source layer thickness at segment ends but a highly variable one at segment centers. The center of hotter and magmatically active segments would be associated with shallow Curie isotherm; hence there is a thin magnetic source layer and a low amplitude; centers of colder segments would be associated with a deeper Curie isotherm, a thicker magnetic source layer, and a higher amplitude (Figure 8). The relationship between ΔA and ΔMBA (Figure 6a) would therefore be verified by this model.

The predicted variations of magnetic source layer thickness depending on the depth of the Curie isotherm among segments result in relatively grouped amplitudes at segment ends and scattered amplitudes at segment centers, in better agreement with the along-axis amplitudes variations of colder segments, i.e., presenting a low ΔMBA (Figure 7d). This result is, of course, strongly dependent on the crude assumption of varying temperatures among segment centers and rather uniform ones at segment ends; however, to make this process in agreement with the along-axis amplitudes variations of hotter segments, i.e., presenting a high ΔMBA (Figure 7c), would require the opposite assumption of varying temperature at segment ends and uniform ones at segment centers, which seems inconsistent with the observed ridge propagations.

The variable magnetic source layer thickness model depending on the Curie isotherm depth would therefore apply to colder segments. However, most thermal models of mid-ocean ridges predict the 300°C isotherm (Curie temperature for titanomagnetite) to be deeper than 1 km within a few kilometers from the ridge axis (see, for instance, *Chen and Morgan* [1990]). Variations of Curie isotherm depth would therefore not significantly affect the whole axial magnetic anomaly, about 30 km wide, but only the most recent part of this anomaly within a narrow zone. Hence variations of Curie isotherm depth may play a significant role in shaping the central magnetic anomaly high observed on most deep-tow magnetic anomaly measurement over the youngest oceanic crust [e.g., *Tivey and Johnson,* 1993; *Tivey,* 1994; *Gee and Kent,* 1994] but cannot explain the systematic amplitude variations observed within and among the segments investigated.

4.2.3. Serpentinization of ultramafic rocks at segment ends. Outcrops of ultramafic rocks have been widely observed in the vicinity of FZ and second-order discontinuities along the MAR [e.g., *Juteau et al.,* 1990; *Cannat et al.,* 1995; *Gente et al,* 1995; *Lagabrielle et al.,* 1998] and are rare (but not absent, see *Lagabrielle et al.* [1998]) at segment centers. These observations suggest that a low magmatic budget, a relatively colder thermal structure, and thin crust prevail at segment ends [e.g., *Cannat,* 1993; *Tisseau and Tonnerre,* 1995]. Shallow (and outcropping) peridotites are easily serpentinized by seawater, a process which generally results in the formation of secondary magnetite (see *Toft et al.* [1990] for a review). As a consequence, most serpentinized peridotites bear high induced and remanent magnetizations [*Bina et al.,* 1990; *Hamano et al.,* 1990; *Nazarova,* 1994]. The presence of such serpentinized bodies in the vicinity of the discontinuities could result in high axial magnetic anomaly amplitudes. The amplitude decrease toward segment center might be a result of the decreasing abundance of shallow (or outcropping) serpentinized material. If serpentinization is the dominant process, geometrical considerations would predict high amplitudes at the center of a short segment and lower amplitudes at the center of a longer segment. As the length of the segments decreases, the presence of serpentinized material in the vicinity of segment centers (supposed to be hotter, see assumptions in section 3.2) is more likely so that any correlation between ΔA and ΔMBA would become less obvious (Figure 8).

These considerations show that serpentinization of ultramafics at segment ends is consistent with the positive correlation between ΔA and ΔMBA (Figure 6a), as the amplitude at segment ends would be rather uniform and the amplitude at segment centers would decrease with longer and hotter segments (increasing ΔMBA). The serpentinization model predicts grouped amplitudes at segment ends and scattered amplitudes at segment centers, in agreement with the along-axis pattern observed for colder segments (i.e., associated with a low ΔMBA, Figure 7d) but not with that observed for hotter segments (Figure 7c). This result suggests that serpentinized peridotites are an important process to generate high axial magnetic anomaly amplitudes at the ends of segment in a relatively colder thermal state (Figure 9), in good agreement with the direct observation of low amount of basalts and abundant ultramafics at the tips of these segments, but may only play a secondary role in the amplitude variations at hotter segments.

4.2.4. Magma shallow fractionation. Although the relationship between fractionation and temperature is complex and depends on other parameters such as magma feeding and composition, it is generally accepted that hotter temperatures correspond to abundant and mixed magma upon ascent and therefore low degree of fractionation and magnetization; conversely, colder temperatures correspond to lower amount of partial melting and high degree of fractionation and magnetization. Such a fractionation effect is clearly observed in the vicinity of large offset FZ and second-order discontinuities [e.g., *Langmuir and Bender,* 1984; *Niu and Batiza,* 1994; *Lawson et al.,* 1996; *Weiland et al.,* 1996; *Fleutelot et al.,* 1996]. Under the assumption of relatively uniform temperatures at segment ends and highly variable temperatures at segment centers (see section 3.2), fractionation may affect the ridge segments in a different way depending on the temperature at segment center. Two classes of segments are envisioned.

The first class of segments includes hotter segments associated with a robust magmatic activity, which present regularly fed magmatic bodies. As ascending magma is focused at the segment centers along slow spreading centers such as the MAR [e.g., *Lin and Phipps Morgan,* 1992], the degrees of fractionation and hence magnetization are low and uniform at segment center and increase

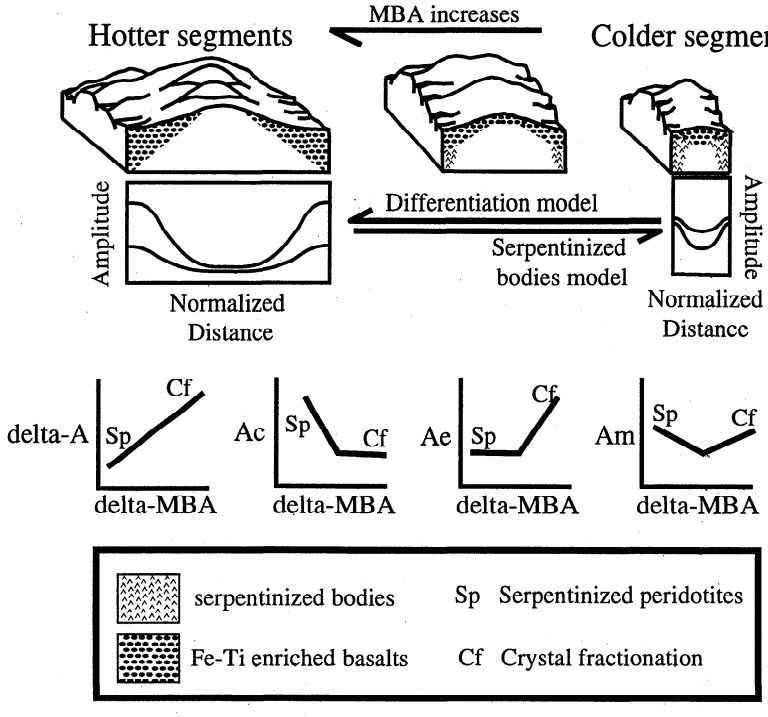

Figure 9. Proposed model accounting for along-axis amplitudes variations among hotter, intermediate, and colder segments. For hotter segments, fractionation results in uniform low amplitudes at segment centers and variable high amplitudes at segment ends (for comparison, see Figure 7c). For colder segments, fractionation at segment centers and serpentinized bodies at segment ends result in uniform and relatively high amplitudes at segment ends and scattered lower amplitudes at segment centers (for comparison, see Figure 7d). Expected relationships linking ΔMBA with ΔA, amplitude at center A_c, amplitude at ends A_e and mean amplitude A_m which result from the combination of these two processes (bottom) are in relatively good agreement with the observations (see Figure 6).

toward segment ends. If these quantities vary similarly in all segments, the longer segments would display the most fractionated magmatic rocks at its ends and hence have the highest Fe-Ti content, magnetization, and axial magnetic anomaly amplitude. For this class of segments, the shallow fractionation model is consistent with the observed variations of ΔA, A_c, A_e and A_m with ΔMBA (Figure 6) and with the observed along-axis amplitudes variations for segments with ΔMBA higher than 25 mGal (Figure 7c) in regard to the rough assumptions considered (Figure 8).

The second class of segments includes colder segments presenting a modest magmatic activity and irregularly fed magmatic bodies which are submitted to longer times of insulation. The degree of fractionation at segment center depends on the temperature and hence the Fe-Ti content, magnetization, and magnetic anomaly amplitude. Thus the axial magnetic anomaly amplitude at segment center would decrease with increasing temperature at segment center and ΔMBA (Figure 8) and is expected to present a large dispersion, as it is indeed observed (Figures 6d and 7d). Similary, the amount of melt decreases and the degree of fractionation increases toward segment ends. The longer segments of this class, associated with a relatively high ΔMBA and low temperatures at segment center, would present a more important variation in degree of fractionation between segment center and ends, which may compensate their lower degree of fractionation at segment center and result in relatively uniform degree of fractionation hence magnetization at segment ends among the segments of this class. For this class of segments, the shallow fractionation model is consistent with the variations of ΔA, A_c, A_e and A_m with ΔMBA (Figure 6). It predicts scattered amplitudes at segment centers and rather uniform amplitudes at segment ends, in agreement with the observation for segments with ΔMBA lower than 18 mGal (Figure 7d). However, fractionation is unrealistic to explain the high axial magnetic anomaly amplitude observed at segment ends where large outcrops of deep crustal and mantle rocks are exposed, basalts are almost absent, and the magmatic budget is very low. In such area, serpentinized ultramafic bodies likely play a major role in the observed amplitude variations (see section 4.2.3 and Figure 9).

Very few systematic studies of FeO* content within segments have been reported, and only a limited number of measurements of this parameter are available along the MAR from the literature. A good example has been recently published by *Lawson et al.* [1996]: segment K14, located immediately north of Kane FZ, shows more primitive lavas at segment center and more

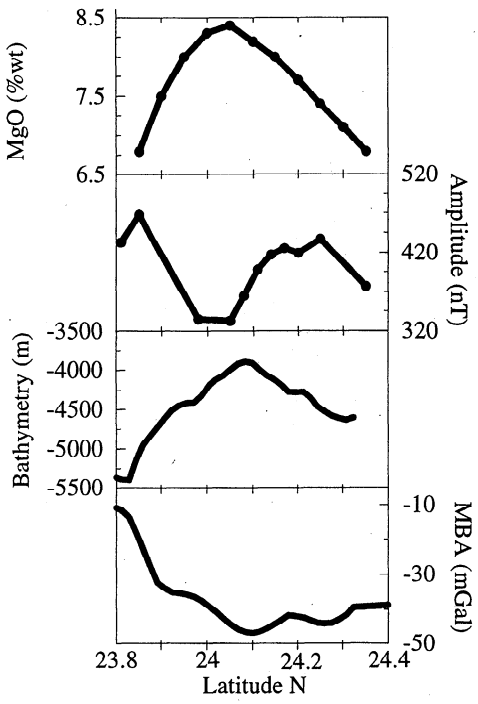

Figure 10. From top to bottom, MgO content [*Lawson et al.*, 1996], axial magnetic anomaly amplitude, bathymetry, and mantle Bouguer gravity anomaly along the segment located immediatly north of Kane FZ (segment KA14). With respect to its ΔMBA, segment KA14 is intermediate between the hotter and the colder state (see Figure 7). The low magnetic anomaly amplitude at segment center corresponds to a high MgO content, i.e., a low FeO content. This good correlation and the comparable asymmetries observed on the four data sets suggest that fractionation is the primary process to explain the variations of axial magnetic anomaly amplitude. The complexities observed in the amplitude variations but not in the MgO content variations may reflect local effects of secondary processes.

fractionated basalts at segment ends, as suggested by MgO variations [*Lawson et al.*, 1996]: a high MgO (i.e., a low FeO, as Mg and Fe concurrently stand at the same sites in molecular structures) is observed at segment center and decreases asymmetrically toward segment ends (Figure 10). Comparison with the axial magnetic anomaly amplitude within this particular segment reveals a clear relationship. The highest MgO (lowest FeO) content corresponds to the lowest axial magnetic anomaly amplitude, and the asymmetric variations of MgO content toward each segment end translate in similar asymmetric variations of the axial magnetic anomaly amplitude (Figure 10). However, the axial magnetic anomaly amplitude shows more complex variations, including local fluctuations of slopes and a slight decrease of the amplitude at the extreme tips of the segment, than the MgO content, which seems much more regular despite a relatively dense sampling.

5. Conclusion

Our systematic study of the axial magnetic anomaly amplitudes along a 2600-km section of the Mid-Atlantic Ridge axis between 20°N and 40°N provides important results at two different scales. The long-wavelength signal (> 100 km) displays two highs of axial magnetic amplitudes centered at 39°N (Azores platform) and at 28°30'N. The 39°N amplitude high is associated with marked bathymetric, gravity, geoid, seismic velocity, and geochemical anomalies. These combined observations likely result for the thermal perturbation associated to the Azores hotspot, which may induce deeper and more extensive partial melting and generate a thick and/or Fe-Ti enriched magnetic source layer in this area, in partial agreement with the magnetic telechemistry hypothesis. The 28°30'N amplitude high is associated to weaker bathymetric and gravity anomalies at the wavelengths of about 400 km and comparable geoid and seismic velocity anomalies. These observations may reflect the presence of a thermal perturbation which would result in locally thicker and/or Fe-Ti enriched magnetic source layer. The presence of long-wavelength bathymetric, gravity, and geoid anomalies centered on the Azores, which are not observed at 28°30'N, suggests a deep thermal anomaly below the Azores hotspot and a relatively shallow one at 28°30'N.

Shorter undulations (< 100 km) of the axial magnetic anomaly amplitude signal are related to ridge segmentation. The joint study of a large number of segments (1) allows us to generalize the observation of higher amplitude at segment ends than at segment centers and (2) provides the opportunity to analyze the variations of axial anomaly amplitudes among segments, by comparison with ΔMBA interpreted as reflecting the thermal state of each segment. Hotter and magmatically active segments display higher along-axis amplitude variations characterized by grouped amplitudes at segment center and scattered amplitudes at segment ends. Conversely, colder and less magmatically active segments show lower along-axis amplitudes variations, scattered amplitudes at segment center, and grouped amplitudes at segment ends. These inferences suggest the following:

1. Low-temperature alteration through faulting and hydrothermal circulation and variable source layer thickness through variations of the Curie isotherm depth may locally affect the amplitude of magnetic signal.

2. Shallow fractionation and serpentinization of ultramafic rocks at segment ends control the amplitude variations within segments. The balance between these processes depends on the thermal state among segments. Amplitude variations within hotter segments are mainly due to fractionation, whereas those displayed by colder segments result from the combined effect of fractionation at segment center and the presence of serpentinized bodies at segment ends.

Acknowledgments. This study was funded by the French program "Dorsales" under the "Appel d'offres: magnétisme des dorsales." M.R. and R.T. acknowledge research fellowships from the French Ministry of Education and Research. We thank C. Croguennec from Sismer, Brest, for kindly and efficiently providing the available data in the study area. We also thank J. L. Thirot for providing the tomographic data, K. Perrot for providing the geoid map shown in Figure 4, and J. Goslin, J.L. Thirot, and O. Noel

for interesting discussions. Comments from M. Tivey, an anonymous reviewer, and Associate Editor P. Wessel resulted in considerable improvement of the paper and are sincerely acknowledged. JD would like to thank T. Fujiwara for a discussion on the difference of axial magnetic anomaly amplitudes at 29°N and 24°N on the Mid-Atlantic Ridge. Softwares GMT (P. Wessel and W.H.F. Smith) and Xmgr (P.J. Turner) were used to produce the figures.

References

Anderson, R.N., D.J. Spariosu, J.K. Weissel, and D.E. Hayes, The interrelation between variations in magnetic amplitudes and basalt magnetization and chemistry along the Southeast Indian Ridge, *J. Geophys. Res., 85,* 3883-3898, 1980.

Argus, D.F., G.G. Gordon, C. DeMets, and S. Stein, Closure of the Africa-Eurasia-North America plate motion circuit and tectonics of the Gloria fault, *J. Geophys. Res., 94,* 5585-5602, 1989.

Arkani-Hamed, J., A.L. Langel, and M. Purucker, Scalar magnetic anomaly maps of Earth derived from POGO and Magsat data, *J. Geophys. Res., 99,* 24,075-24,090, 1994.

Bina, M.M., B. Henry, and M. Cannat, Magnetic anisotropy and some other magnetic properties of serpentinized peridotites from ODP hole 670A, *Proc. Ocean Drill. Program Sci. Results, 106-109,* 263-267, 1990.

Bleil, U., and N. Petersen, Variations in magnetization intensity and low-temperature titanomagnetite oxidation of ocean floor basalts, *Nature, 301,* 384-388, 1983.

Bonatti, E., Not so hot spots in the oceanic mantle, *Science, 250,* 107-111, 1990.

Calvert, A.J., Seismic evidence for a magma chamber beneath the slow-spreading Mid-Atlantic Ridge, *Nature, 377,* 410-414, 1995.

Cannat, M., Emplacement of mantle rocks in the seafloor at mid-ocean ridges, *J. Geophys. Res., 98,* 4163-4172, 1993.

Cannat, M., How thick is the magmatic crust at slow spreading oceanic ridges?, *J. Geophys. Res., 101,* 2847-2857, 1996.

Cannat, M., C. Mével, M. Maia, C. Deplus, C. Durand, P. Gente, P. Agrinier, A. Belarouchi, G. Dubuisson, E. Humler, and J. Reynolds, Thin crust, ultramafic exposures, and rugged faulting patterns at the Mid-Atlantic Ridge [22°-24°N], *Geology, 23,* 49-52, 1995.

Carbotte, S., and K.C. Macdonald, East Pacific Rise 8°-10°30'N: Evolution of ridge segments and discontinuities from SeaMARC II and three-dimensional magnetic studies, *J. Geophys. Res., 97,* 6959-6982, 1992.

Cazenave, A., P. Schaeffer, M. Berge, C. Brossier, K. Dominh, and M.C. Gennero, High-resolution mean sea surface computed with altimeter data of ERS-1 (geodetic mission) and Topex-Poseidon, *Geophys. J. Int., 125,* 696-704, 1996.

Chen, Y., and W.J. Morgan, A nonlinear rheology model for mid-ocean ridge axis topography, *J. Geophys. Res., 95,* 15583-15604, 1990.

Christie, D.M., and J.M. Sinton, Evolution of abyssal lavas along propagating segments of the Galapagos spreading center, *Earth Planet. Sci. Lett., 56,* 321-335, 1981.

Detrick, R.S., and W.S. Lynn, The origin of high- amplitude magnetic anomalies at the intersection of the Juan de Fuca Ridge and Blanco Fracture zone, *Earth Planet. Sci. Lett., 26,* 105-113, 1975.

Detrick, R.S., J. Collins, R. Stephen, and S. Swift, In situ evidence for the nature of the seismic layer 2/3 boundary in oceanic crust, *Nature, 370,* 288-290, 1994.

Detrick, R.S., H.D. Needham, and V. Renard, Gravity anomalies and crustal thickness variations along the Mid-Atlantic Ridge between 33°N and 40°N, *J. Geophys. Res., 100,* 3767-3787, 1995.

Dosso, L., H. Bougault, and J.L. Joron, Geochemical morphology of the north Mid-Atlantic Ridge, 10°- 24°N: Trace element-isotope complementarity, *Earth Planet. Sci. Lett., 120,* 443-462, 1993.

Dunlop, D.J., and C.J. Hale, Simulation of long-term changes in the magnetic signal of the oceanic crust, *Can. J. Earth Sci., 14,* 716-744, 1977.

Dyment, J., and J. Arkani-Hamed, Spreading-rate-dependent magnetization of the oceanic lithosphere inferred from the anomalous skewness of marine magnetic anomalies, *Geophys. J. Int., 121,* 789-804, 1995.

Dyment, J., J. Arkani-Hamed, and A. Ghods, Contribution of serpentinized ultramafics to marine magnetic anomalies at slow and intermediate spreading centres: Insights from the shape of the anomalies, *Geophys. J. Int., 129,* 691-701, 1997.

Fleutelot, C., J.P. Eissen, T. Tonnerre, L. Danyushevsky, V. Rory, L. Mollard, T. Juteau, J. Cotten, and M. Bohn, Propagation d'accrétion en contexte arrière-arc: premiers résultats de la campagne ProFeTi (Bassin Nord Fidjien, Pacifique SO), *C. R. Acad. Sci. Ser.I , 322,* 853-860, 1996.

Fouquet, Y., J.L. Charlou, I. Costa, J.P. Donval, J. Radford-Knoery, H. Pelle, H. Ondreas, N. Lourenco, M. Segonzac, and M.K. Tivey, A detailed study of the Lucky Strike hydrothermal site and discovery of a new hydrothermal site: Menez Gwen; preliminary results of the Diva 1 cruise (5-29 may 1994), *InterRidge News, 3,* 14-17, 1994.

Freire Luis, J., J.M. Miranda, A. Galdeano, P. Patriat, J.C. Rossignol, and L.A. Mendes Victor, The Azores triple junction evolution since 10 Ma from an aeromagnetic survey of the Mid-Atlantic Ridge, *Earth Planet. Sci. Lett., 125,* 439-459, 1994.

Fujimoto, H., W. Bryan, T. Matsumoto, and K. Kobayashi, MODE 94 Shinkai 6500 dives in WMARK area on the Mid-Atlantic Ridge, *Cruise report of the fleet of JAMSTEC for Deep Sea Research,* vol. 2, 141 p., Jp. Mar. Sci. Technol. Cent., Yokosuka, Japan, 1996.

Furuta, T., Magnetic properties and ferromagnetic mineralogy of oceanic basalts, *Geophys. J. Int., 113,* 95-114, 1993.

Gay, S.P., Jr., Srandard curves for interpretation of magnetic anomalies over long tabular bodies, *Geophysics, 28,* 161-200, 1963.

Gee, J., and D.V. Kent, Variations in layer 2A thickness and the origin of the central anomaly magnetic high, *Geophys. Res. Lett., 21,* 297-300, 1994.

Geiss, E., N. Petersen, and U. Bleil, Amplitude variation of marine magnetic anomalies, *Geol. Rundsch., 78,* 741-752, 1989.

Gente, P., Segmentation et formation des reliefs des dorsales: implications sur les processus de l'accrétion, thèse d'habilitation, Univ. de Bretagne Occidentale, France, 1995.

Gente, P., R.A. Pockalny, C. Durand, C. Deplus, M. Maia, G. Ceuleneer, C. Mevel, M. Cannat, and C. Laverne, Characteristics and evolution of the Mid-Atlantic Ridge between 20°and 24°N during the last 10 million years, *Earth Planet. Sci. Lett., 129,* 55-71, 1995.

Grindlay, N.R., P.J. Fox, and P.R. Vogt, Morphology and tectonics of the Mid-Atlantic Ridge (25°-27°30'S) from Sea Beam and magnetic data, *J. Geophys. Res., 97,* 6983-7010, 1992.

Hamano, Y., M.M. Bina, and K. Krammer, Paleomagnetism of serpentinized peridotites from ODP hole 670A, *Proc. Ocean Drill. Program Sci. Results, 106-109,* 257-262, 1990.

Hussenoeder, S.A., M.A. Tivey, H. Schouten, and R.C.

Searle, Near-bottom magnetic survey of the Mid- Atlantic Ridge axis, 24°-24°40'N: Implications for crustal accretion at slow spreading ridges, *J. Geophys. Res., 101,* 22,051-22,069, 1996.

IAGA Division V Working Group 8, Revision of International Geomagnetic Reference Field released, *Eos Trans. AGU, 77,* 153, 1996.

Johnson, H.P., and J.E. Pariso, Variations in oceanic crustal magnetization: Systematic changes in the last 160 million years, *J. Geophys. Res., 98,* 435-445, 1993.

Juteau, T., M. Cannat, and Y. Lagabrielle, Serpentinized peridotites in the upper oceanic crust away from transform zones: A comparison of the results of previous DSDP and ODP legs, *Proc. Ocean Drill. Program, Sci. Results, 106-109,* 303-308, 1990.

Klein, E.M., and C.H. Langmuir, Global correlations of ocean ridge basalts chemistry with axial depth and crustal thickness, *J. Geophys. Res., 92,* 8089-8115, 1987.

Klein, E.M., and C.H. Langmuir, Local versus global variations in ocean ridge basalt composition: A reply, *J. Geophys. Res., 94,* 4241-4252, 1989.

Lagabrielle, Y., and M. Cannat, Alpine Jurassic ophiolites resemble the modern central Atlantic basement, Geology, 18, 319-322, 1990.

Lagabrielle, Y., D. Bideau, M. Cannat, J.A. Karson, and C. Mével, Ultramafic-mafic plutonic rock suite exposed along the Mid-Atlantic Ridge (10°N-30°N): Symmetrical-asymmetrical distribution and implications for seafloor spreading processes, in AGU, Geophysical Monograph Series, edited by W.R. Buck, J.R. Delaney, and J.A. Karson, Washington, D.C., in press, 1998.

Langmuir, C.H., and J.F. Bender, The geochemistry of oceanic basalts in the vicinity of transform faults: Observations and implications, *Earth Planet. Sci. Lett., 69,* 107-127, 1984.

Langmuir, C.H., et al., Geological setting and characteristics of the Lucky Strike vent field at 37°17'N on the Mid-Atlantic Ridge, *Eos Trans. AGU, 74* (43), Fall Meet. Suppl., 99, 1993.

Lawson, K., R.C. Searle, J.A. Pearce, P. Browning, and P. Kempton, Detailed volcanic geology of the MARNOK area, Mid-Atlantic Ridge north of Kane transform, in *Tectonic, Magmatic, Hydrothermal and Biological Segmentation of Mid-Ocean Ridges,* edited by C.J. MacLeod, P.A. Tyler, and C.L. Walker, *Geol. Soc. Spec. Publ., 118,* 61-102, 1996.

Lin, J., and J. Phipps Morgan, The spreading rate dependence of three-dimensional mid-ocean ridge gravity structure, *Geophys. Res. Lett., 19,* 13-16, 1992.

Lin, J., G.M. Purdy, H. Schouten, J.C. Sempéré, and C. Zervas, Evidence for focused magmatic accretion along the Mid-Atlantic Ridge, *Nature, 344,* 627-632, 1990.

Macdonald, K.C., Near-bottom magnetic anomalies, asymmetric spreading, oblique spreading, and tectonics of the Mid-Atlantic Ridge near lat 37°N, *Geol. Soc. Am. Bull., 88,* 541-555, 1977.

McGregor, B.A., C.G.A. Harrison, J.W. Lavelle, and P.A. Rona, Magnetic anomaly patterns on Mid-Atlantic Ridge crest at 26°N, *J. Geophys. Res., 82,* 231-238, 1977.

Melson, W.G., and T. O'Hearn, Basaltic glass erupted along the Mid-Atlantic Ridge between 0°-37°N: Relationships between composition and latitude, in *Deep Drilling Results in the Atlantic Ocean: Ocean Crust, Maurice Ewing Ser.,* vol.2, edited by M. Talwani, C.G. Harrison, and D.E. Hayes, pp. 249-261, *AGU, Washington, D.C.,* 1979.

Morel, J.M., and R. Hekinian, Compositional variations of volcanics along segments of recent spreading ridges, *Contrib. Mineral. Petrol., 23,* 38-52, 1980.

Murton, B.J., G. Klinkhammer, C.L. VanDover, K. Becker, A. Briais, D. Edge, N. Hayward, M. Eudnicki, K. Sayanagi, H. Sloan, and L. Parson, Direct evidence for the distribution and occurrence of hydrothermal activity between 27°N-30°N on the Mid-Atlantic Ridge, *Earth Planet. Sci. Lett., 125,* 119-128, 1994.

Mutter, C.Z., and J.C. Mutter, Variations in thickness of layer 3 dominate oceanic crustal structure, *Earth Planet. Sci. Lett., 117,* 295-317, 1993.

Nazavora, K.A., Serpentinized peridotites as possible source for oceanic magnetic anomalies, *Mar. Geophys. Res., 16,* 455-462, 1994.

Niu, Y., and R. Batiza, Magmatic processes at a slow-spreading ridge segment: 26°S Mid-Atlantic Ridge, *J. Geophys. Res., 99,* 19,719-19,740, 1994.

O'Connors, J.M., and R.A. Duncan, Evolution of the Walvis Ridge-Rio Grande Rise hot spot system: Implications for African and South American plate motion over plumes, *J. Geophys. Res., 95,* 17,475- 17,502, 1990.

Pariso, J.E., and H.P. Johnson, Do layer 3 rocks make a significant contribution to marine magnetic anomalies? In situ magnetization of gabbros at Ocean Drilling Program hole 735B, *J. Geophys. Res., 98,* 16,033-16,052, 1993.

Pariso, J.E., C. Rommevaux, and J.C. Sempéré, Three-dimensional inversion of marine magnetic anomalies: Implications for crustal accretion along the Mid-Atlantic Ridge (28°-31°30'N), *Mar. Geophys. Res., 18,* 85-101, 1996.

Parker, R.L., The rapid calculation of potential anomalies, Geophys. *J. R. Astron. Soc., 31,* 447-455, 1972.

Parker, R.L., and S.P. Huestis, The inversion of magnetic anomalies in the presence of topography, *J. Geophys. Res., 79,* 1587-1596, 1974.

Pockalny, R.A., A. Smith, and P. Gente, Spatial and temporal variability of crustal magnetization of a slowly spreading ridge: Mid-Atlantic Ridge (20°- 24°N), *Mar. Geophys. Res., 17,* 301-320, 1995.

Ranalli, G., Seismic tomography and mineral physics, in *Seismic Modelling of Earth Structure,* edited by E. Boshi, G. Ekström, and A. Morelli, pp. 443-461, Compositori, Bologna, Italy, 443-461, 1996.

Ravat, D., R.A.Langel, M. Purucker, J. Arkani-Hamed, and D.E. Alsdorf, Revised vector and scalar Magsat magnetic anomaly maps, *J. Geophys. Res., 100,* 20,111-20,136, 1995.

Rona, P.A., Magnetic signatures of hydrothermal alteration and volcanogenic mineral deposits in oceanic crust, *J. Volcanol. Geotherm. Res., 3,* 219-225, 1978.

Sandwell, D.T., and W.H.F. Smith, Marine gravity anomaly from Geosat and ERS-1 satellite altimetry, *J. Geophys. Res., 102,* 10,039-10,054, 1997.

Sayanagi, K., and K. Tamaki, Long-term variations in magnetization intensity with crustal age in the northeast Pacific, Atlantic, and southeast Indian Oceans, *Geophys. Res. Lett., 19,* 2369-2372, 1992.

Schilling, J.G., Geochemical and isotopic variation along the Mid-Atlantic Ridge axis from 79°N to 0°N, in *The Geology of North America,* vol. M, *The Western North Atlantic region,* edited by P.R. Vogt and B.E. Tucholke, pp. 137-156, *Geol. Soc. of Am.,* Boulder, Colo., 1986.

Schilling, J.G., R.N. Anderson, and P.R. Vogt, Rare earth, Fe and Ti variations along the Galapagos spreading center, and their relationship to the Galapagos mantle plume, *Nature, 261,* 108-113, 1976.

Schilling, J.G., M. Zajac, R. Evans, T. Johnson, W. White, J. Devine, and R. Kingsley, Petrologic and geochemical variations along the Mid-Atlantic Ridge from 29°to 73°N, *Am. J. Sci.,* 510-586, 1983.

Schouten, H., and K. McCamy, Filtering marine magnetic anomalies, *J. Geophys. Res., 77,* 7089-7099, 1972.

Schultz, N., R. Detrick, and S. Miller, Two and three dimensional inversions of magnetic anomalies in the MARK

area (Mid-Atlantic Ridge 23°N), *Mar. Geophys. Res., 10,* 41-57, 1988.

Sempéré, J.C., High-magnetization near spreading center discontinuities, *Earth Planet. Sci. Lett., 107,* 389-405, 1991.

Sempéré, J.C., G.M. Purdy, and H. Schouten, Segmentation of the Mid-Atlantic Ridge between 24°N and 30°40'N, *Nature, 344,* 427-431, 1990.

Sempéré, J.C., J. Lin, H.S. Brown, H. Schouten, and G.M. Purdy, Segmentation and morphotectonic variations along a slow-spreading ridge (24°00'N-30°40'N), *Mar. Geophys. Res., 15,* 153-200, 1993.

Sigurdsson, H., First order major element variation in basalts glasses from the Mid-Atlantic Ridge: 29 to 73°N, *J. Geophys. Res., 86,* 9483-9502, 1981.

Su, W.J., and A.M. Dziewonski, Predominance of long-wavelengthheterogeneity in the mantle, *Nature, 352,* 121-126, 1991.

Thibaud, R., P.Gente, and M. Maia, A systematic analysis of the Mid-Atlantic Ridge morphology and gravity between 15°N and 40°N: Contraints of the thermal structure, *J. Geophys. Res.,* this issue.

Tisseau, C., and T. Tonnerre, Non steady state thermal model of spreading ridges: Implications for melt generation and mantle outcrops, in *Mantle and Lower Crust Exposed in Oceanic Ridges and in Ophiolites,* edited by R.L.M. Vissers and A. Nicolas, pp. 181-214, Kluwer, Norwell, Mass, 1995.

Tivey, M.A., Fine scale magnetic anomaly field over the southern Juan de Fuca Ridge: Axial magnetization low and implications for crustal structure, *J. Geophys. Res., 99,* 4833-4855, 1994.

Tivey, M.A., and H.P. Johnson, The central magnetic anomaly high: Implications for ocean crust construction and evolution, *J. Geophys. Res., 92,* 12,685-12,694, 1987.

Tivey, M.A., and H.P. Johnson, Variations in oceanic crustal structure and implications for the fine-scale magnetic anomaly signal, *Geophys. Res. Lett., 20,* 1879-1882, 1993.

Tivey, M.A., P.A. Rona, and H. Schouten, Reduced crustal magnetization beneath the active sulfide mound, TAG hydrothermal field, Mid-Atlantic Ridge at 26°N, *Earth Planet. Sci. Lett., 115,* 101-105, 1993.

Tivey, M.A., P.A. Rona, and M.C. Kleinrock, Reduced crustal magnetization beneath relict hydrothermal mounds: TAG hydrothermal field, Mid-Atlantic Ridge, 26°N, *Geophys. Res. Lett., 23,* 3511-3514, 1996.

Toft, P.B., J. Arkani-Hamed, and S.E. Haggerty, The effects of serpentinization on density and magnetic susceptibility: A petrophysical model, *Phys. Earth Planet. Inter., 65,* 137-157, 1990.

Tolstoy, M., A.J. Harding, and J.A. Orcutt, Crustal thickness on the Mid-Atlantic Ridge: bull's-eye gravity anomalies and focused accretion, *Science, 262,* 726-729, 1993.

Vogt, P.R., Amplitudes of oceanic magnetic anomalies and the chemistry of oceanic crust: synthesis and review of magnetic telechemistry, *Can. J. Earth Sci., 16,* 2236-2262, 1979.

Vogt, P.R., and J. de Boer, Morphology, magnetic anomalies, and basalt magnetization at the ends of the Galapagos high-amplitude magnetic zone, *Earth Planet. Sci. Lett.,* 33, 145-163, 1976.

Vogt, P.R., and G.L. Johnson, Magnetic telechemistry of oceanic crust, *Nature, 245,* 373-375, 1973.

Vogt, P.R., B. Zondek, P.W. Fell, N.Z. Cherkis, and R.K. Perry, Seasat altimetry, the North Atlantic geoid, and evaluation of shipborne subsatellite profiles, *J. Geophys. Res., 89,* 9885-9903, 1984.

Weiland, C.M., and K.C. Macdonald, Variation of crustal magnetization at the Mid-Atlantic Ridge 31°-36°S: Rock magnetism and 3-dimensional inversion, *Eos Trans. AGU, 74* (16), Spring Meet. Suppl., 304, 1993.

Weiland, C.M., K.C. Macdonald, and N.R. Grindlay, Ridge segmentation and the magnetic structure of the southern Mid-Atlantic Ridge 26°S and 31°-35°S: Implications for magmatic processes at slow spreading centers, *J. Geophys. Res., 101,* 8055-8073, 1996.

Wittpenn, N.A, C.G.A. Harrison, and D.W. Handschumacher, Crustal magnetization in the South Atlantic Ocean from inversion of magnetic anomalies, *J. Geophys. Res., 94,* 15,463-15,480, 1989.

Wooldridge, A.L., S.E. Haggerty, P.A. Rona, and C.G.A. Harrison, Magnetic properties and opaque mineralogy of rocks from selected seafloor hydrothermal sites at oceanic ridges, *J. Geophys. Res., 95,* 12,351-12,374, 1990.

Wooldridge, A.L., C.G.A. Harrison, M.A. Tivey, and P.A. Rona, Magnetic modeling near selected areas of hydrothermal activity on the Mid-Atlantic and Gorda Ridges, *J. Geophys. Res., 97,* 10,911-10,926, 1992.

Zhang, Y.S., and T. Tanimoto, Ridges, hotspots and their interaction as observed in seismic velocity maps, *Nature, 355,* 45-49, 1992.

J. Dyment, P. Gente, M. Ravilly, and R. Thibaud, CNRS UMR "Domaines Océaniques", Institut Universitaire Européen de la Mer, Université de Bretagne Occidentale, 1 place Nicolas Copernic, Technopole Brest-Iroise, 29280 Plouzané, France. (e-mail: jerome@univ-brest.fr)

(Received April 1, 1997; revised March 1, 1998;
accepted March 24, 1998.)